Thermohydraulic assessment of mixing behaviors and entropy generation using pseudoplastic fluids in short microfluidic devices

Embarek Douroum [a,b]*, Amar Kouadri [a], Sofiane Khelladi [c], Samir Laouedj [b], Abdelylah Benazza [b].

[a] Renewable Energy Systems Applications Laboratory, LASER, University of Djelfa 17000, Algeria
[b] Laboratory of materials and reactive systems, LMSR, Djillali Liabes University, Sidi Bel Abbes 22000, Algeria
[c] Arts et Metiers Institute of Technology, CNAM, LIFSE, HESAM University, F-75013 Paris, France

***Corresponding author:** embarek.douroum@univ-djelfa.dz (Embarek Douroum)

Abstract:

Thermal mixing fluids in chaotic microdevices have significant importance in many potential applications and have enormous utility in thermal engineering processes. In microfluidic devices, The Two-Layer with Crossing Channels Micromixer (TLCCM) emphasized its efficiency in thermally homogenizing Newtonian fluids, which inspired us to investigate its performance using pseudoplastic fluids. A numerical comparative investigation has been carried out to evaluate the thermal mixing performances of pseudoplastic fluids in laminar steady flows using four chaotic microdevices: TLCCM, L, OH and OX. Quantitative validation of pseudoplastic fluids within a complex geometry, subject to constant heat flux, has been done. Navier-Stokes, the mass conservation, energy and species transport equations have been solved numerically employing CFD code. The pseudoplastic fluids consist of carboxymethyl cellulose solutions, which are characterized using the power-law model, the flow behavior index ranging from 0.75 to 1 and the generalized Reynolds number ranging from 0.2 to 70. To quantify the thermal mixing efficiency, the effects of the fluid behavior index, the generalized Reynolds number, on the thermal mixing degree for the proposed micromixers are presented, where high thermal mixing degrees have been obtained which evolve between 0.9 and 0.99. The entropy generation due to heat transfers and fluid pressure drops has been introduced versus the generalized Reynolds numbers for different fluid behaviour indexes. The Bejan number values evolve close to 1. The probability density function PDF (%) at the TLCCM micromixer exit is localized in a narrow range that refers to the ideal temperature value for mixing, which is 315 Kelvin, whatever the fluid behavior index value.

Keywords : Microfluidic devices, pseudoplastic fluids, Thermal mixing degree, Entropy generation, Bejan number.

1. Introduction

The study of fluid mixing with heat transfer is always of great interest to industrialists. Among the industries which have recourse to mixing operations, lots of applications can be cited: nuclear field, Droplet and emulsion processes, chemical reactors, Extraction and purification processes, Biological analysis, cosmetics, polymer processing…etc. [1−7]. The mixing actually tends to improve the homogeneity of the fluids in contact where the different areas of the fluid are reoriented, stretched and folded, which increases the gradient of the scalar in the fluid by the creation of increasingly thin layers. In the case of very viscous fluids of a non-Newtonian nature, the classical methods of turbulent mixing can be costly in terms of energy and destructive of the physical properties of these fluids. Moreover, the properties or consistency of some delicate liquids may be negatively affected when exposed to flows that cause too much shear stress, for instance, this applies to various biological liquids and polymer solutions composed of extended molecular structures. In such cases, the use of mixing by chaotic advection is a better alternative, and it has shown its effectiveness for the mixing of a scalar field (concentration, temperature) for very viscous fluids in microfluidics [8−10].

Since the 90s, many researchers have investigated using chaotic advection as a method to enhance thermal homogenizing. The research on using chaotic advection for thermal mixing can be categorized into two essential modes: active mode which involving rotating elements such as cylinders [11−~~14~~15], and passive mode for those involving a succession of complex channels [~~15~~16−~~17~~19]. The second class of flow corresponds to continuous mixing processes with 2D or 3D flows that do not require moving parts.

In order to obtain better thermal mixing for non-Newtonian fluids, several works have exploited potential chaotic microfluidic devices to assess their fluid flow behavior and heat transfer capabilities in the state of non-Newtonian fluids. The effects of the generalized Reynolds number, the fluid behavior index, and the sidewall effect of the microdevices geometry are presented and analyzed in these works. Srisamran et al. [~~18~~20] have conducted computational simulations involving non-Newtonian pseudo-plastic fluids to assess the mixing characteristics of steady, two-dimensional, laminar fluids in closed geometries. The study analyzed the impacts of varying parameters, such as the inlet jet Reynolds numbers varied from 10 to 200, and the fluid behavior index from 0.6161 to 1, regarding the resulting flow patterns and mixing effectiveness. The temperature variation of the combining liquids was utilized as an indicator to examine the mixing homogeneity. Both empirical studies and computational simulations have been conducted by Mendels et al. [~~19~~21], to determine the water concentration in a methanol/water-methanol mixing and the thermal mixing in a T-junction micromixer. Two different temperatures have been considered at the inlets of 30 and 60°C with a flow rate equal to 10 ; 25 ; 50 ; 75 $\mu l \cdot min^{-1}$. The combination of fluorescence imaging microscopy (FLIM) and CFD have been used to measure the thermal diffusion coefficients. Their results illustrate that the process of mixing and heat transfer could be attributed to the interaction between two mixing mechanisms: diffusion and advection. In a numerical study, Mashaei et al. [~~20~~22] have analyzed the thermohydraulic characteristics of non-Newtonian fluid mixing in a 2D T-junction micromixer. Their results demonstrated that increasing the Reynolds number and fluid behavior index led to improved thermal mixing enhancement. Nevertheless, the thermal mixing degree along the channel rises as the fluid behavior index rises. The angle of the T-junction has minimal influence on the thermal mixing along the channel, however, increasing the impact angle can enhance the mixing. Luo et al. [~~21~~23] have conducted direct numerical simulations of a square cross-section T-junction micromixer, using both Newtonian and non-Newtonian fluid models. Their findings show that for pseudo-plastic fluids, the mixing is promoted more efficiently in the "impinging regime" than in the "deflecting regime". Thus a distinct flow structure is found between the "deflecting regime" and the "impinging regime". Maurya et al. [~~22~~24] performed a computational investigation on laminar, stationary flow through a 2D T-junction micromixer. They investigated the effects of Reynolds numbers (10 − 50), fluid behavior indexes (0.6161 − 1), and the difference in temperature (ΔT = 10 K) on the mixing characteristics of pseudo-plastic fluids. Their results showed that an elevated mixing index could be achieved over a short distance with an elevated fluid behavior index (n = 1) but at weak values of Reynolds number. However, in the interaction area, the mixing index decreased rapidly. Additionally, they noticed that the Nusselt number and temperature difference exhibited minimal impact on the mixing efficiency.

Entropy generation is an energy degradation that occurs when energy is transformed into heat or exchanged between two fluid species at different temperatures. The entropy generation related with fluid flow is driven by viscous and thermal mechanisms, involving gradients in velocity and temperature. The thermal mixing performance within the micromixers, encompassing various flow types, is intricately tied to the minimization of entropy generation and therefore this narrow localization serves as a compelling impetus to gain deeper insight into the various mechanisms underpinning entropy generation. Optimal configurations for thermodynamic systems have been extensively suggested through the lens of the second law of thermodynamics [~~23~~25]. To enhance the heat exchange efficiency of Newtonian fluids in micromixers, the entropy generation rate must be effectively controlled. Bejan [~~24~~26] has presented a method

for calculating entropy in a flow field and have proposed a principle for generating minimum entropy. The entropy generation and second law analysis of thermodynamics for laminar flow in a straight channel have been investigated by Yilbas et al. [~~25~~27] have developed dimensionless variables to quantify the heat transfer, the entropy generation, and the irreversibility. The findings reveal that irreversibility increases with higher Prandtl numbers. Zimparov [~~26~~28] has formulated extended performance criteria, grounded in the entropy increase associated with heat exchange across surfaces maintained at constant temperature.

The improvement of heat transfer occurring within a thermal system is invariably accompanied by increases in pressure losses. The analysis of irreversibility in various complex geometries for Newtonian fluids with constant imposed heat flux on the wall and with a laminar flow has been carried out by Sahin [~~27~~29] and Sahin [~~28~~30] as well as the optimization of helical serpentine channels or double sinusoidal channels which have been performed by Ko [~~29~~31] and Ko et al. [~~30~~32]. These latter have studied the entropy generation using a CFD code for the pseudo-plastic fluids flow in a curved and heated rectangular pipe. The influences of three parameters, which are the Dean number, the heat flux through the external walls and the cross-sectional aspect ratio, have been presented on the entropy generated by the irreversibility (pressure drops and heat transfer). Their findings indicate that for flow conditions with a high Dean number and low wall heat flux, the major contributor to entropy generation is irreversibility from pressure drop. On the other hand, for flows with a low Dean number and high wall heat flux, the entropy generation is primarily driven by irreversibilities associated with heat transfer. Zimparov et al. [~~31~~33] have enhanced the efficiency of different categories of fully established laminar flow, in T-junction and Y-junction micromixers, maximum thermal efficiency is realized by minimizing entropy generation for each geometry. Kurnia et al. [~~32~~34] have assessed the heat transfer efficiency and entropy generation characteristics of laminar flow through six different geometric configurations of straight and helical tubes with similar cross-sections. Several parameters have been examined: the geometry shape, the wall temperature, the Reynolds number and the heating/cooling mode as well as the relationship between the heat transfer rate and the required pumping power. Their findings showed that compared to straight tubes, coiled tube geometries achieved a higher rate of heat transfer while also having a lower rate of entropy generation, while the square section produces the maximum entropy, with the ellipse and circle following. Yang et al. [~~33~~35] have carried out numerical simulations to characterize the thermohydraulic performances using carboxymethylcellulose (CMC) solutions in microchannels with four different structural designs, across varying flow rates and CMC concentrations. Their results indicated that the finned microchannel geometry offered the most uniform temperature distribution, and a CMC concentration of 2000 ppm was the recommended aqueous solution. At low flow rates, grooved microchannels were preferred, while V-grooved shapes demonstrated the lowest relative entropy generation, thereby achieving superior thermal performance at elevated flow rates. Kaood et al. [~~34~~36] have performed a computational investigation to assess the heat transfer and entropy generation behaviors when using convergent tubes with several dimple patterns on the surface, exposed to a constant heat flux condition. Their findings illustrated that the dimple pattern had a substantial impact on the heat transfer and entropy generation efficiency. The convergent tubes with a stepped-conical dimple pattern achieved the highest average thermal enhancement factor, representing a 7.81% improvement compared to a smooth reference tube.

Inspired by the research of Xia et al. [~~35~~37], who proposed the foremost important passive microdevices for Newtonian fluids mixing, which allowed them to obtain good mixing at low flow rates. The micromixer investigated by Kouadri et al [~~36~~38,~~37~~39] consisting of two layers crossing channels with a length of 7.5 mm, their findings showed that the micromixer is more efficient in Newtonian and non-Newtonian fluids mixing. Then Kouadri et al [~~38~~40] and Douroum et al [~~39~~41,~~40~~42], invented an improved model of the TLCCM micromixer with a compact length of 3.75 mm and obtained high mixing performance similar to that of double length micromixers.

In this work, the TLCCM microdevice exploited previously for the thermo-hydraulic mixing of Newtonian fluids is used exclusively for the thermo-hydraulic mixing of non-Newtonian pseudo-plastic fluids across vast range of generalized Reynolds number (0.1-70) with fluid behavior index ranges from 0.75 to 1. Numerical simulations of two fluids mixing with different inlet temperatures within TLCCM micromixer and three others: L, OH and OX micromixers were carried out. The thermal mixing performances of the considered micromixers were analyzed and compared. The investigation of entropy generation linked to heat transfers and pressure drops made it possible to evaluate the irreversibility of heat exchanges and to interpret the thermal mixing performances of the different studied micromixers.

2. Geometrical models of studied micromixers

Four geometric models of micromixers have been analyzed, with their primary dimensions illustrated in Fig. 1. This figure highlights various features of the studied micromixers and indicates where mixing quality is evaluated. Fig. 1(a) presents a three-dimensional view of the TLCCM micromixer, showing its two inlets and a single outlet. The micromixer's key dimensions are as follows: the channel width (W) is 300 µm, the height of each layer (d) is 150 µm, the overall micromixer width (H) is 1070 µm, the transversal channel width (b) is 150 µm, the step size (S) is 640 µm, and the length of each mixing unit (b + S) is 790 µm. The inlet sections measure 150 × 300 µm, while the outlet section is 300 × 300 µm. The total length of the micromixer spans 3750 µm.

The hydraulic diameter is a key parameter in micromixer design, defined by a specific formula: $D_h = \frac{2d \cdot W}{d+W}$

To evaluate the effectiveness of the TLCCM micromixer for pseudoplastic fluids mixing, it is compared against three recently studied designs. These comparative micromixers are constructed with identical hydraulic diameters of 200 µm and equivalent total lengths of 3750 µm. Fig. 1(b), (c), and (d) provide three-dimensional views of these proposed micromixers, labeled as L, OH, and OX, along with their respective dimensions. This consistent sizing across all models allows for a fair comparison of their mixing efficiencies.

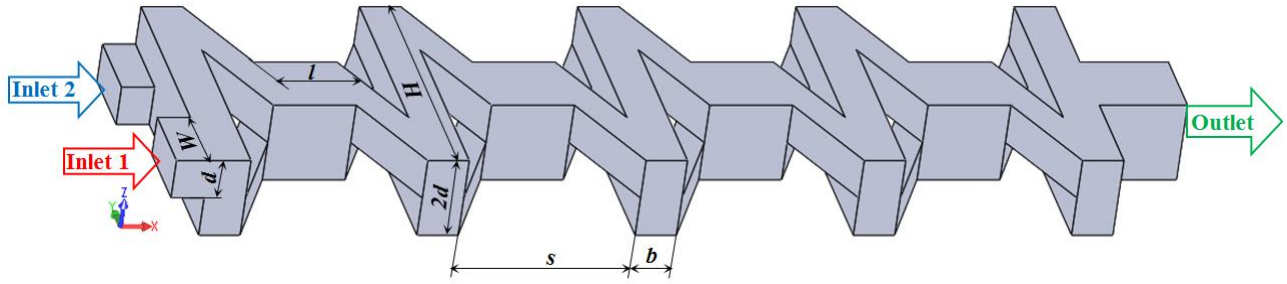

(a)

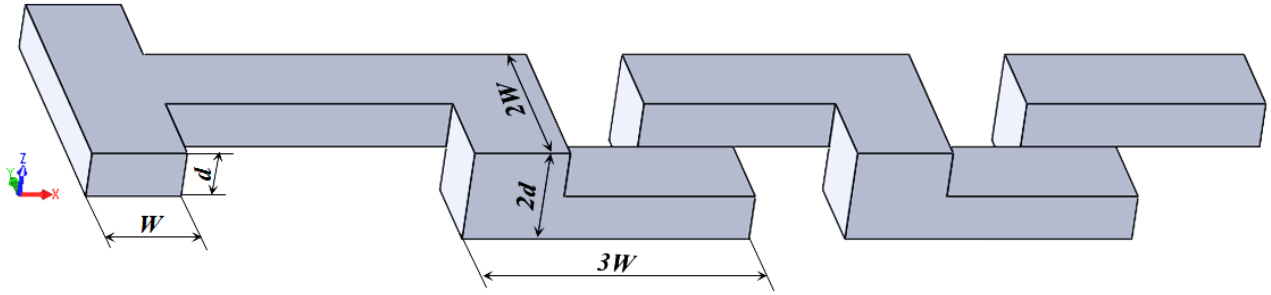

(b)

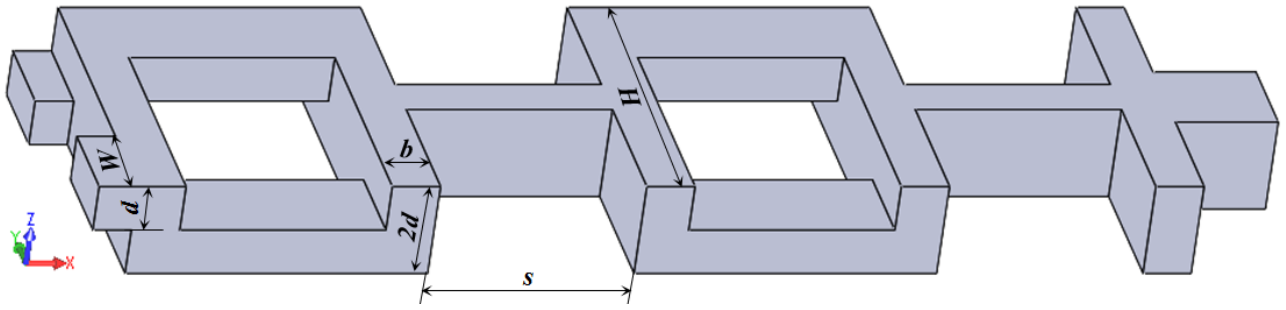

(c)

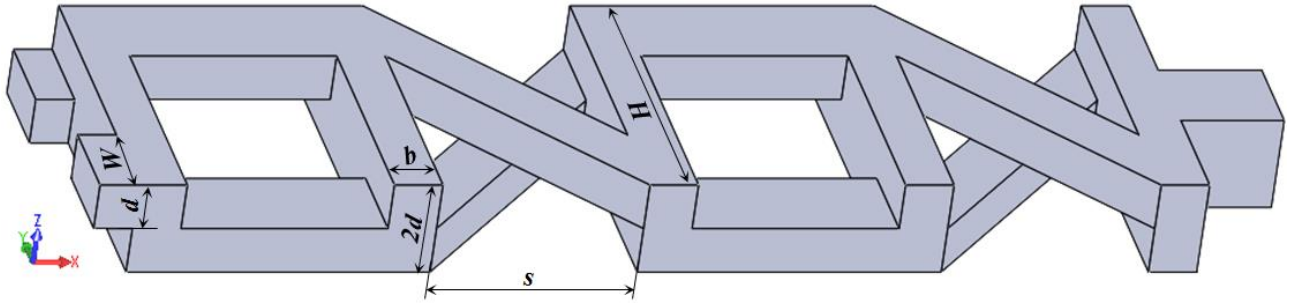

(d)

Fig. 1. Designs of studied micromixers: (a) TLCCM; (b) L; (c) OH; (d) OX.

3. Mathematical formulations and numerical methods

This section presents the fundamental equations and associated boundary conditions governing the system under study. It includes the formulation of the generalized Reynolds number and defines all parameters used to evaluate thermal mixing performance. Additionally, it describes the specific mixing model chosen for the analysis. These mathematical foundations and numerical approaches form the basis for understanding and quantifying the micromixer behavior and effectiveness.

3.1. Mathematical formulation

The numerical simulations for this study were performed using the ANSYS Fluent software package. The behavior of three-dimensional, incompressible, and steady-state flows is described by a set of governing equations. These equations begin with the continuity equation, which is represented by Equations (Eq 1 and 2), momentum equation involving the tensor of shear stress (Eq 3, 4, 5, and 6), and energy equation (Eq 7 and 8). These equations are expressed as fellow:

$$\nabla.\vec{V} = 0 \tag{1}$$

Which could be expressed by:

$$\frac{\partial \mathrm{u}}{\partial \mathrm{x}} + \frac{\partial \mathrm{v}}{\partial \mathrm{y}} + \frac{\partial \mathrm{w}}{\partial \mathrm{z}} = 0 \tag{2}$$

$$\rho\left(\vec{V}\cdot\nabla\right)\vec{V} = -\nabla \mathrm{P} + \nabla\cdot\bar{\bar{\tau}} \tag{3}$$

That can be represented in expanded notation as:

$$\left(u\frac{\partial u}{\partial x} + v\frac{\partial u}{\partial y} + w\frac{\partial u}{\partial z}\right) = -\frac{1}{\rho}\frac{\partial P}{\partial x} + \frac{1}{\rho}\left[\frac{\partial \tau_{xx}}{\partial x} + \frac{\partial \tau_{xy}}{\partial y} + \frac{\partial \tau_{xz}}{\partial z}\right] \tag{4}$$

$$\left(u\frac{\partial v}{\partial x} + v\frac{\partial v}{\partial y} + w\frac{\partial v}{\partial z}\right) = -\frac{1}{\rho}\frac{\partial P}{\partial y} + \frac{1}{\rho}\left[\frac{\partial \tau_{yx}}{\partial x} + \frac{\partial \tau_{yy}}{\partial y} + \frac{\partial \tau_{yz}}{\partial z}\right] \tag{5}$$

$$\left(u\frac{\partial w}{\partial x} + v\frac{\partial w}{\partial y} + w\frac{\partial w}{\partial z}\right) = -\frac{1}{\rho}\frac{\partial P}{\partial z} + \frac{1}{\rho}\left[\frac{\partial \tau_{zx}}{\partial x} + \frac{\partial \tau_{zy}}{\partial y} + \frac{\partial \tau_{zz}}{\partial z}\right] \tag{6}$$

The energy equation is written as follows:

$$\rho c\vec{V}.\nabla T = \lambda\nabla^2 T \tag{7}$$

The developed notation of the energy equation is given by:

$$\left(u\frac{\partial T}{\partial x}+v\frac{\partial T}{\partial y}+w\frac{\partial T}{\partial z}\right)=\frac{1}{\rho c}\left[\frac{\partial}{\partial x}\left(\lambda\frac{\partial T}{\partial x}\right)+\frac{\partial}{\partial y}\left(\lambda\frac{\partial T}{\partial y}\right)+\frac{\partial}{\partial z}\left(\lambda\frac{\partial T}{\partial z}\right)\right] \quad (8)$$

In the mathematical notation used, the symbols represent key physical quantities in fluid dynamics. Specifically, V stands for velocity, ρ represents density, P denotes static pressure, and $\bar{\bar{\tau}}$ symbolizes the shear stress tensor. These concise notations allow for efficient expression of complex fluid behavior within the equations governing the micromixer system. And in the energy equation (Eq 8): the quantities c, T, and λ represent respectively, the calorific heat capacity, fluids temperature, and the thermal conductivity.

For equations (Eq 4, 5, and 6), τ_{ij} denotes the viscous tensor of shear stresses, for a pseudo-plastic fluid, according to the power-law model, shear stress tensor is expressed by:

$$\tau_{ij}=\mu_{app}\varepsilon_{ij} \quad (9)$$

where μ_{app} and ε_{ij} denote in the respective order the apparent viscosity and the strain rate tensor, which can be written as:

$$\varepsilon_{ij}=\frac{\partial u_i}{\partial x_j}+\frac{\partial u_j}{\partial x_i} \quad (10)$$

The power-law model, also known as the Ostwald De-Waele model, is particularly effective in characterizing the viscosity of pseudoplastic fluids (where $n < 1$) within a specific range of shear rates. This model is preferred over alternatives due to its ability to accurately represent the behavior of working fluids in confined shear rate intervals. Its widespread adoption in research is largely attributed to its straightforward nature, making it a practical choice for many studies in fluid dynamics.

$$\tau=m\dot{\gamma}^n \quad (11)$$

The fluid consistency coefficient is represented by "m", while "n" signifies the fluid behavior index. Using these parameters, we can express the apparent viscosity of the fluid with the following equation:

$$\mu_{app}=m\dot{\gamma}^{n-1} \quad (12)$$

where $\dot{\gamma}$ represents the shear rate which is given by:

$$\dot{\gamma}=\sqrt{\frac{\left(\varepsilon_{ij}:\varepsilon_{ij}\right)}{2}}=\sqrt{\frac{I_2}{2}} \quad (13)$$

The symbol I_2 represents the second invariant of the strain rate tensor. This invariant is directly related to the apparent viscosity μ_{app} of the fluid through the following equation:

$$\mu_{app}=m\left(\frac{I_2}{2}\right)^{\frac{n-1}{2}} \quad (14)$$

with:

$$\frac{I_2}{2}=2\left(\frac{\partial u}{dx}\right)^2+2\left(\frac{\partial v}{\partial y}\right)^2+2\left(\frac{\partial w}{\partial z}\right)^2+\left(\frac{\partial u}{\partial y}+\frac{\partial v}{\partial x}\right)^2+\left(\frac{\partial u}{\partial z}+\frac{\partial w}{\partial x}\right)^2+\left(\frac{\partial v}{\partial z}+\frac{\partial w}{\partial y}\right)^2 \quad (15)$$

ANSYS Fluent offers a range of models for characterizing mixing. The species transport model is commonly used for mixing miscible fluids, taking into account the mass diffusion coefficient.

The CFD (Computational Fluid Dynamics) software models fluid mixing and species movement by solving conservation equations for each individual species. These equations account for both convection and diffusion processes. The calculations ensure that the sum of mass fractions for all species "i" always equals 1.

The conservation equation of the fluid species is defined as:

$$\nabla\cdot\left(\rho\vec{V}C_i\right)=-\nabla\cdot\vec{J_i} \quad (16)$$

Here, J_i represents the mass diffusion flux for the fluid species. This flux depends on concentration and pressure gradients, which drive the diffusive motion during mixing. The computational code incorporates the dilute approximation, based on Fick's law, to model mass diffusion. The mass diffusion flux is given by:

$$\vec{J_i} = -D_i \nabla(\rho C_i) \tag{17}$$

where D_i is the coefficient of mass diffusion of species "i".

Therefore, the species transport equation is given by:

$$(\vec{V} \cdot \nabla) C_i = D_i \nabla^2 C_i \tag{18}$$

This equation is expressed in Cartesian coordinates with the following expanded form:

$$u\frac{\partial C_i}{\partial x} + v\frac{\partial C_i}{\partial y} + w\frac{\partial C_i}{\partial z} = D_i\left(\frac{\partial^2 C_i}{\partial x^2} + \frac{\partial^2 C_i}{\partial y^2} + \frac{\partial^2 C_i}{\partial z^2}\right) \tag{19}$$

The diffusion coefficient D_i is assumed to be 3.6×10^{-10} m^2/s for the pseudoplastic fluids (Das et al. [~~41~~43]). Additionally, the mixing process is governed by the mechanism of chaotic advection.

The simulation employs the following boundary conditions:

- Wall boundaries: A no-slip condition is applied, setting all velocity components (U, V, W) to zero.
- Fluid inlets: Both inlets are assigned uniform velocities (U = constant). The mass fraction distribution is set as follows:
  - Inlet 1: 100% fluid 1, 0% fluid 2.
  - Inlet 2: 0% fluid 1, 100% fluid 2.
  - Outlet: Atmospheric pressure is specified.
- Thermal conditions:
  - Hot fluid temperature: 330 K.
  - Cold fluid temperature: 300 K.
  - Wall heat transfer: All walls are treated as adiabatic (δQ = 0), preventing heat exchange with the surroundings.

3.2. Fluid characteristics

For modeling non-Newtonian pseudo-plastic fluid flows, CMC (carboxymethyl cellulose) solutions are employed. As suggested by Srisamran et al. [~~18~~20], the density of these solutions is assumed to be 1000 kg/m³. The rheological properties of the CMC solutions, specifically the consistency coefficient and the fluid behavior index, are detailed in Table 1.

Table 1.

Rheological properties of carboxymethyl cellulose solutions as described by Pinho et al. [~~42~~44], and Fellouah et al. [~~43~~45]

CMC concentration (%)	Fluid behavior index *n* (-)	coefficient of consistency *m* (Pa.s^n)
0.000	1.000	0.000902
0.100	0.930	0.006600
0.200	0.850	0.025200
0.250	0.750	0.097000
0.700	0.490	2.750000

The thermal conductivity and heat capacity of working fluids are shown in table 2.

Table 2.

Thermodynamic characteristics of working fluids.

Thermal conductivity	Density	Heat capacity
0.6069 W/m.K	1000 kg/m^3	4 181.7 J/Kg.K

3.3. Characterization of the mixing performance

To highlight the thermal mixing efficiency of the considered micromixers, we focus on the thermal mixing degree (TMD), entropy generation and the probability density function (PDF). These quantities allow us to quantify the enhancement in the thermal mixing performance of the considered micromixers.

3.3.1. Thermal mixing degree (TMD)

The thermal mixing degree (TMD) of two fluids (cold and hot) is an adequate parameter to quantitatively evaluate the thermal mixing performance. It's given by the expression bellow:

$$TMD = 1 - \frac{\sqrt{\frac{1}{N}\sum_{i=1}^{N}(T_i - \bar{T})^2}}{\sigma_0} \tag{23}$$

where N is the number of cells in each cross section, T_i is the temperature at every node i, $\bar{T}$ is the average temperature of the cross sectional plane, and σ_0 is the maximum standard deviation at the entrance section. *TMD* values range from zero (not mixed case) to 1 (for fully mixed case).

3.3.2. Probability Density Function *PDF*

The Probability Density Function PDF (%), expressed as a percentage, indicates the likelihood of the scalar temperature T falling within a specific range. At the exit, the PDF for an interval [T_a, T_b] is computed as follows:

This calculation determines the proportion of exit cross-section nodes with temperatures in the given range, providing a statistical representation of temperature distribution at the outlet.

3.3.3. Thermodynamic characterization of heat exchanges

The local entropy generation linked to heat transfer irreversibility (represented as S_T''') and fluid friction irreversibility (represented as S_P''') for a three-dimensional flow are determined based on the temperature and velocity distribution of the flow field (Ko et al., [29,30]):

$$S_T''' = \frac{\lambda}{T^2}\left[\left(\frac{\partial T}{\partial x}\right)^2 + \left(\frac{\partial T}{\partial y}\right)^2 + \left(\frac{\partial T}{\partial z}\right)^2\right] \tag{24}$$

$$S_P''' = \frac{\mu_{app}}{T}\left[2\left(\left(\frac{\partial u}{\partial x}\right)^2 + \left(\frac{\partial v}{\partial y}\right)^2 + \left(\frac{\partial w}{\partial z}\right)^2\right) + \left(\frac{\partial u}{\partial y} + \frac{\partial v}{\partial x}\right)^2 + \left(\frac{\partial u}{\partial z} + \frac{\partial w}{\partial x}\right)^2 + \left(\frac{\partial v}{\partial z} + \frac{\partial w}{\partial y}\right)^2\right] \tag{25}$$

The global entropy generation inside the flow field could be expressed by:

$$S_{gen}''' = S_T''' + S_P''' \tag{26}$$

The average entropy generation $S_{av,gen}'''$ is the sum of the two average entropy generation rates: $S_{av,T}'''$ (linked to heat transfer) and $S_{av,P}'''$ (linked to fluid flow interactions). The whole system of entropy generation equations is defined by:

$$S_{av,T}''' = \frac{1}{V}\int S_T''' dV \tag{27}$$

$$S_{av,P}''' = \frac{1}{V}\int S_P''' dV \tag{28}$$

$$S'''_{av,gen} = \frac{1}{V}\int S'''_{gen} dV \quad (29)$$

where, V is the geometry volume.

Bejan number is expressed as the ratio between the entropy generation linked to the heat transfer and the global entropy generation (Ko et al., [2931,3032]), it can be given by:

$$\mathrm{Be} = \frac{S'''_T}{S'''_{gen}} \quad (30)$$

The Bejan value varies from 0 to 1. Which are the two limit values representing the irreversibility linked to fluid friction and heat transfer respectively.

The average Bejan number ($\mathrm{Be_{av}}$) is given by:

$$\mathrm{Be_{av}} = \frac{S'''_{av,T}}{S'''_{av,gen}} \quad (31)$$

3.4. Expression of the generalized Reynolds number

Determining the flow nature is crucial as it dictates the dominant phenomena. The primary indicator for flow regime prediction is the Reynolds number, which represents the ratio of inertial forces to viscous forces. For pseudoplastic fluids, viscosity changes with strain rate. This necessitates a generalized Reynolds number formulation that accounts for the fluid's rheological behaviors. While various expressions for generalized Reynolds numbers exist in literature for different cross-sections (circular, rectangular, elliptical, etc.), Delplace et al. [4446] proposed a unique formulation. Their expression applies to both Newtonian and pseudoplastic fluids in rectangular cross-sections, regardless of aspect ratio. This formula allows for meaningful comparisons across different flow behavior indices and geometries. The generalized Reynolds number is defined as:

$$\mathrm{Re_g} = \frac{\rho \bar{u}^{2-n} D_h^n}{m\{(24n+\xi)/(24+\xi)n\}^n \xi^{n-1}} \quad (32)$$

where $\bar{u}$ is the average flow velocity, while ξ represents the dimensionless geometric factor.

Table 3.

Empirical values of geometric factor ξ as a function of different aspect ratios α^*.

α^*	0.25	0.5	0.75	1.0
ξ	9.116	7.774	7.238	7.113

In this study, the selected value of the geometric factor ξ related with the aspect ratio α^* as: $\alpha^* = \frac{d}{W} = 0.5$; $\xi = 7.774$.

3.5. Numerical Methodology

This section covers our computational approach, including: an overview of the numerical method, description of the chosen numerical strategy, explanation of the numerical discretization scheme, and a presentation of the mesh independence study used to determine the optimal grid for the micromixers under investigation.

3.5.1 Numerical discretization approach

Our study employs a second-order discretization method to achieve accurate results efficiently while minimizing computational time. Key aspects of our approach include:

- Discretization scheme: A second-order upwind scheme is used for convection terms in the momentum, energy, and species transport equations. This ensures accurate and reliable predictions of mixing performance.

- Pressure-velocity coupling: The SIMPLEC (Semi-Implicit Method for Pressure-Linked Equations-Consistent) algorithm is implemented to achieve convergence and solution stability.
- Convergence acceleration: Under-relaxation factors set at 0.3 are applied for pressure correction, enhancing convergence speed.
- Convergence criterion: Iterative calculations are considered converged when residual values fall below 10^{-6}.

This methodology balances accuracy and computational efficiency in our numerical simulations.

3.5.2 Grid sensitivity test

To determine the optimal cell size and ensure accurate results, a mesh independence analysis was conducted using an unstructured, uniform mesh consisting of tetrahedral cells. The test case selected for this analysis was the TLCCM Micromixer. Four different grid sizes were evaluated, ranging from 221 000 to 1 068 000 cells. The purpose of this analysis was to verify that the simulation results remained consistent and were not significantly affected by further mesh refinement, thereby identifying the most efficient grid resolution for accurate computations.

In this case, Reynolds number is set to 30 and n = 1. The variations of the standard deviation on various cross-sections throughout the micromixer for several mesh grids are illustrated in Fig. 2. It's evident that the trend of the curve for the mesh grid with 637 022 cells closely resembles that of the mesh grid with 1 069 680 cells. While the mesh of 221 643 cells has less computation time and the obtained mixing is more homogeneous which is due to the numerical diffusion. For the mesh of 1 069 680 cells, the computation time is the highest and the obtained mixing degree is very close to that obtained with the mesh of 637 022 which has less computation time.

The analysis led to the selection of a grid containing 637 022 cells. Independence testing showed that this grid, featuring 16 µm cells, offered a good balance between accuracy and computational efficiency. Sensitivity tests, as illustrated in Fig. 3, confirmed the optimal grid sizes for other micromixer designs. For the TLCCM and OX micromixers, which incorporate sharp angles, an unstructured uniform mesh of tetrahedral elements was used. In contrast, the L and OH micromixers were modeled using a structured uniform mesh composed of hexahedral elements.

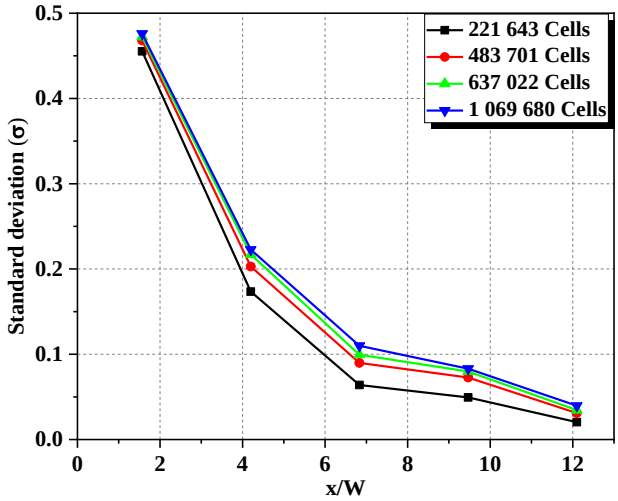

Fig. 2. Mesh sensitivity test by evolutions of standard deviation throughout TLCCM micromixer.

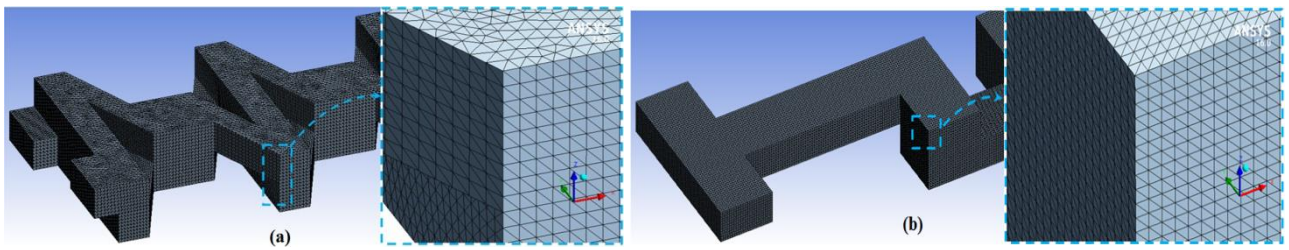

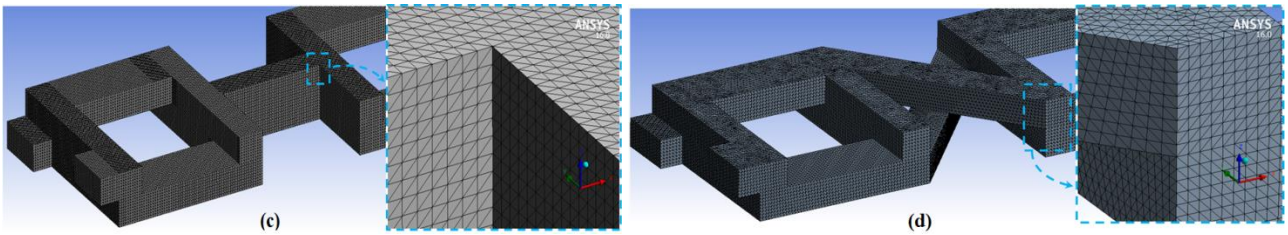

Fig. 3. Mesh grids created for various micromixers with zoomed views: (a) TLCCM, (b) L, (c) OH, and (d) OX.

4. Results and discussion

This study evaluates the effectiveness of previously studied chaotic micromixers, originally designed for Newtonian fluids, in mixing non-Newtonian fluids. The research examines how these micromixers perform with pseudo-plastic fluids, focusing on three key factors: the generalized Reynolds number, the fluid behavior index, and the micromixer wall characteristics. By analyzing these elements, the study aims to assess and improve mixing outcomes for non-Newtonian fluids in these micromixer designs.

4.1. Numerical and experimental validation of CFD code

A numerical quantitative validation was carried out to assess and emphasize the reliability of the numerical simulation findings with those found by Li et al., [~~45~~47]. These results illustrate the heat transfer coefficient versus the generalized Reynolds number. The comparison is satisfying and demonstrates the good agreement between our findings and those of Li et al., [~~45~~47] which are presented in Fig. 3. This demonstrates the precise alignment of our results, obtained from the CFD code simulation, with those of Li et al., [~~45~~47], thus affirming their reliability.

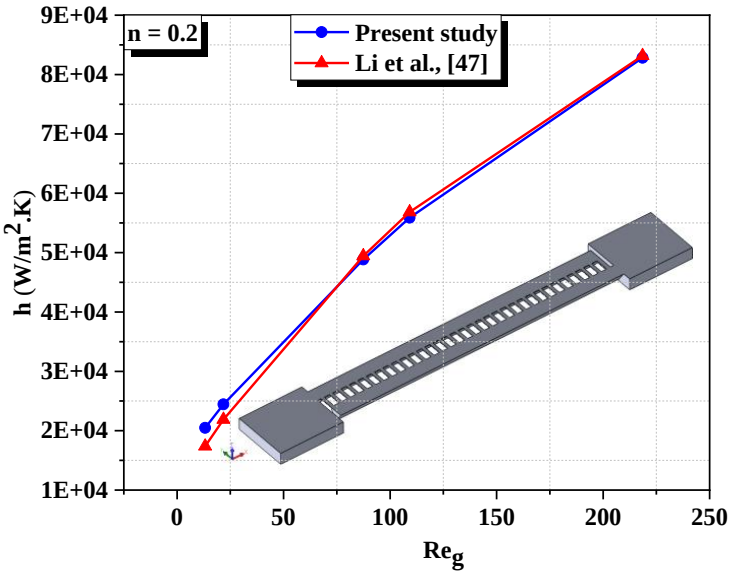

Fig. 4. Comparison of heat transfer coefficient for pseudoplastic fluids flow with Li et al., [~~45~~47].

To ensure the accuracy of the CFD model, we compared its predictions with existing experimental data. Specifically, we examined the mixing degree at the TLCCM micromixer's exit for Reynolds numbers ranging from 0.2 to 120. These computational results were then compared to the experimental findings reported by Hossain et al. [~~46~~48], as shown in Fig. 5. The comparison revealed a strong correlation between the two datasets, with the trends closely aligning. The maximum discrepancy between numerical and experimental results was found to be 4.59%. Any variations observed fell within the expected margin of error for the numerical method employed, thus validating the CFD model's reliability.

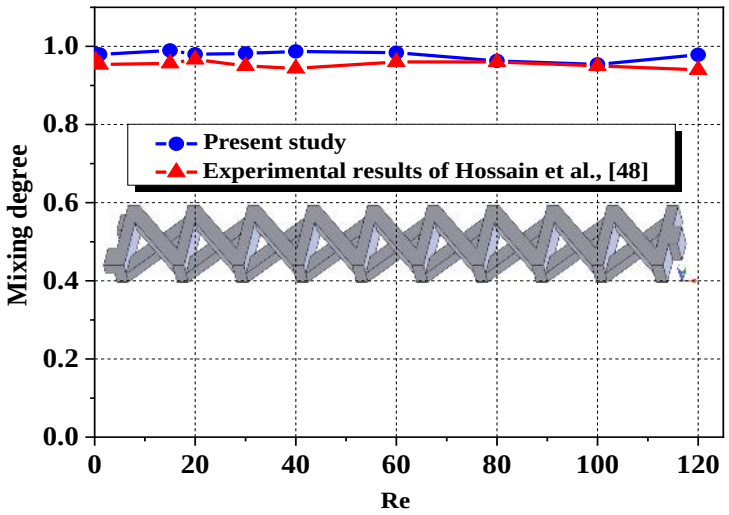

Fig. 5. Comparison of the mixing degree with previous experimental results of Hossain et al., [~~46~~48].

4.2. Thermo-hydraulic mixing behaviors of TLCCM micromixer

The laminar regime can be divided into two distinct sub-regimes: the diffusion regime and the chaotic advection regime. The diffusion regime occurs at very low generalized Reynolds numbers, while the chaotic advection regime is associated with comparatively higher Reynolds number values. Fig. 6 and Fig. 7 show the temperature distribution contours in the three cross-section planes of each crossing elongation (the entrance, the middle and the exit of the crossing).

For Re_g = 1 which represents the molecular diffusion regime where it is seen that the two fluids in the first crossing are separated by a thin layer which widens as n increases and diffuses to occupy the entire outlet section of the first crossing for n = 1. It's also noticed that a significant improvement in the quality of the thermal mixing for all the fluid behavior indexes has been remarked in the second crossing. Moreover, for n = 0.75 and n = 0.85 small zones of different temperatures appeared while the thermal mixing becomes more homogeneous for the 3rd and the 4th crossings throughout the range of the fluid behavior index.

While for Re_g = 30, the temperature distribution contours undergo evolutions illustrated by rotation, compression and stretching, these variations are explained by chaotic advection phenomenon. According to Fig. 6 and for Re_g = 1, As the flow passes through each crossing, the temperature contours exhibit subtle changes in their shape. This mild deformation contributes to improved thermal mixing, which is primarily driven by molecular diffusion. It can be seen from Fig. 7 that the layers of temperature contours undergo significant deformation, precisely between the inlet and the center of the crossing where the temperature contours make from the first crossing a rotation of 90° and then a rotation of 45° in the crossing outlet. Furthermore, in the second crossing, the temperature contours have undergone intense deformations where the thermal mixing becomes more homogeneous, particularly for Newtonian fluids (n = 1), the separation layer is observed to expand, transforming into a mixing region characterized by two distinct, detached cells at the crossing's exit. By the third and fourth crossings, these temperature cells fade away, particularly in Newtonian fluids (where n = 1). This phenomenon explains the noticeable improvement in thermal mixing quality starting from the third crossing onward.

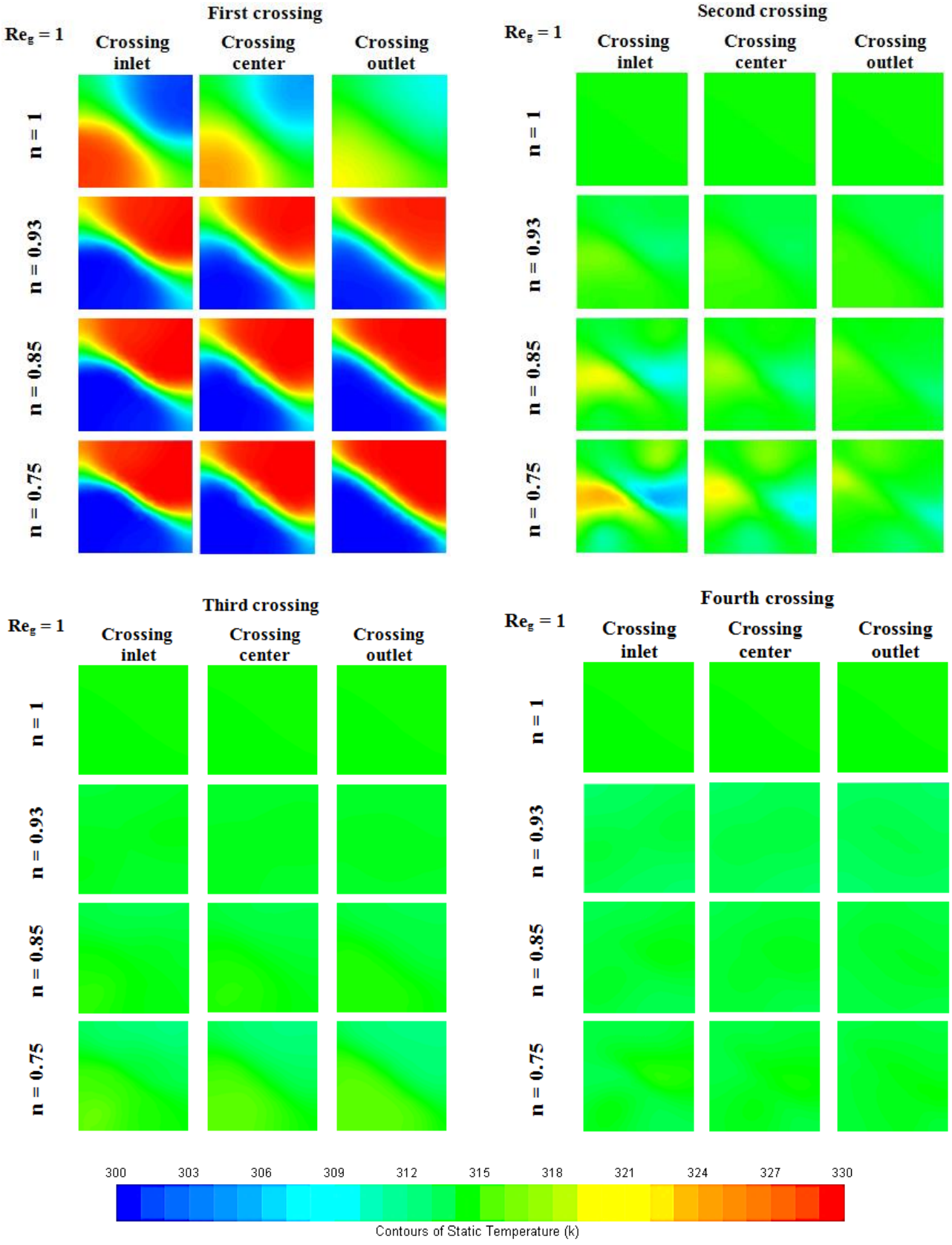

Fig. 6. Temperature distribution contours at several cross sections for several fluid behavior index with $Re_g = 1$.

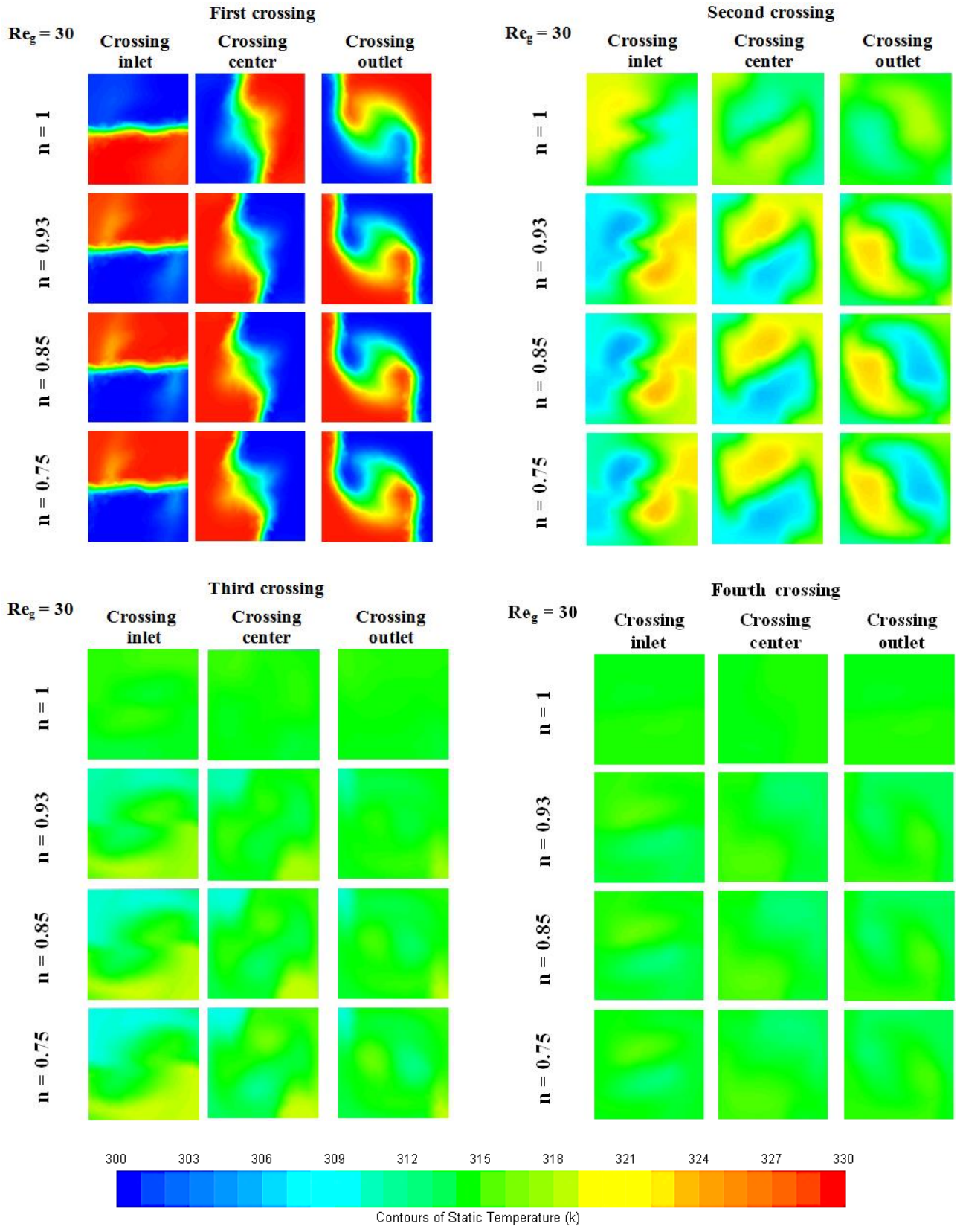

Fig. 7. Temperature distribution contours at several cross sections for several fluid behavior index with $Re_g = 30$.

It's crucial to achieve homogeneous thermal mixing throughout TLCCM micromixer with a fast transport process. These two phenomena typically work against each other: higher flow rates (transport) often reduce the residence time needed for effective mixing, and vice versa. Fig. 8 illustrates how the thermal mixing degree and flow rate at the micromixer exit change with the fluid behavior index, covering a range from 0.75 to 1. Within this range, the flow

shows significant variations even at identical generalized Reynolds numbers. For example, at Re_g = 1, a pseudo-plastic fluid (n = 0.75) flows 22 times faster than a Newtonian fluid (n = 1). In micromixers, faster flow means less time for mixing, resulting in lower thermal mixing efficiency. This explains the reduced thermal mixing observed in pseudo-plastic fluids. Conversely, as the fluid behavior index increases, the flow rate decreases. This extended residence time leads to more homogeneous mixing.

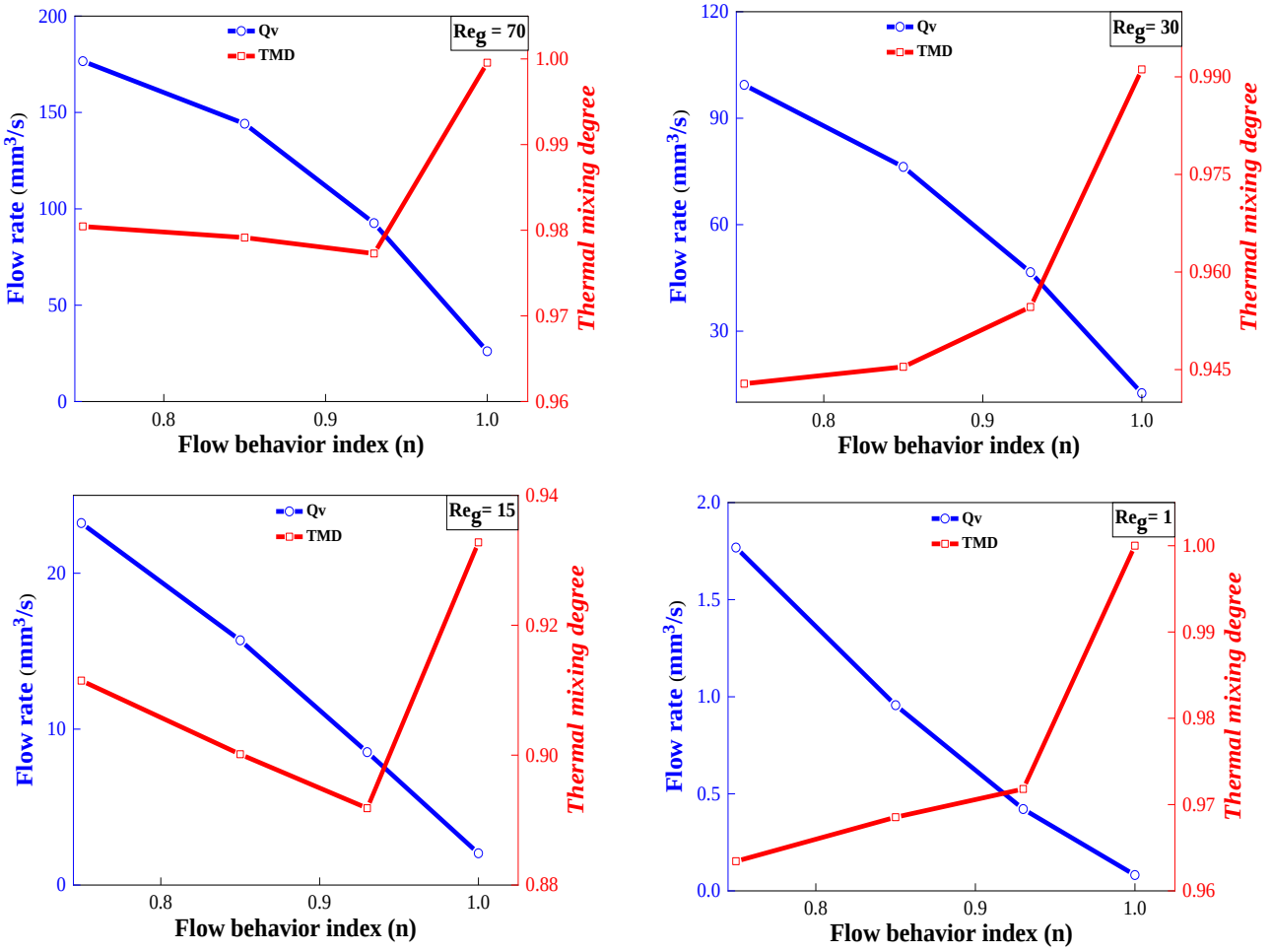

Fig. 8. Changes in Thermal Mixing Degree (TMD) and flow rate at the exit of the TLCCM micromixer, shown for various fluid behavior indices (0.75, 0.85, 0.93, and 1).

4.3 Thermal mixing performances of proposed micromixers

According to the work of Douroum et al., [39] in the state of pseudo-plastic fluids mixing, TLCCM micromixer has elevated thermo-hydraulic mixing efficiencies versus the other studied micromixers. In this study, it's interesting to carry out a comparison of TLCCM thermal mixing performances with those of the other considered micromixers using non-Newtonian fluids. Fig. 9 and Fig. 10 present the evolution of thermal mixing degree throughout the studied micromixers for four values of generalized Reynolds number, and for two extreme cases of fluid behavior index (n = 0.75 and 1). According to these figures, the thermal mixing degree develops progressively throughout TLCCM micromixer for Newtonian and non-Newtonian pseudo-plastic fluids. It's remarkable that a better quality of thermal mixing is recorded with TLCCM micromixer, especially for non-Newtonian fluids (n = 0.75).

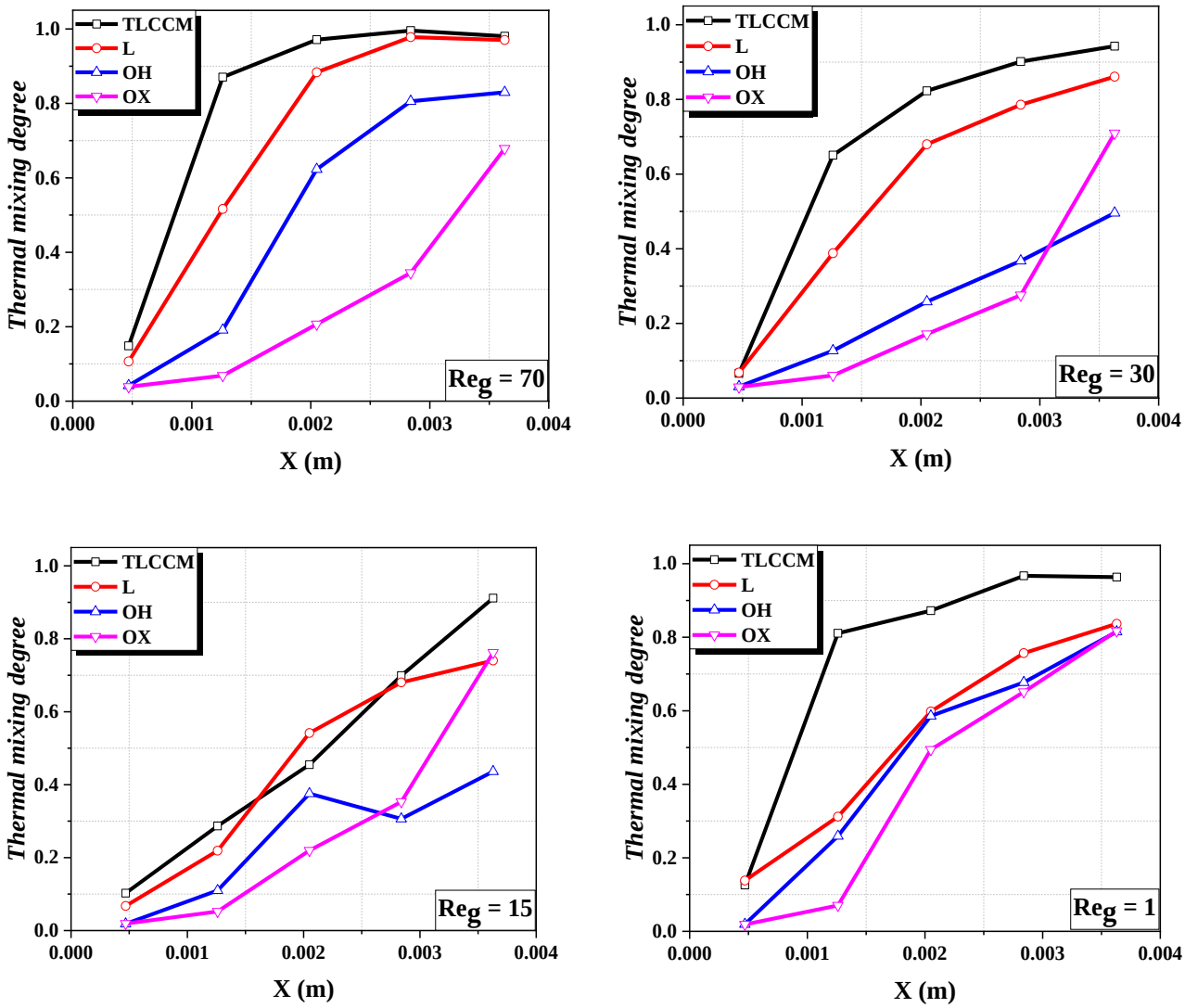

Fig. 9. Developments of the thermal mixing degree throughout the considered micromixers for n = 0.75.

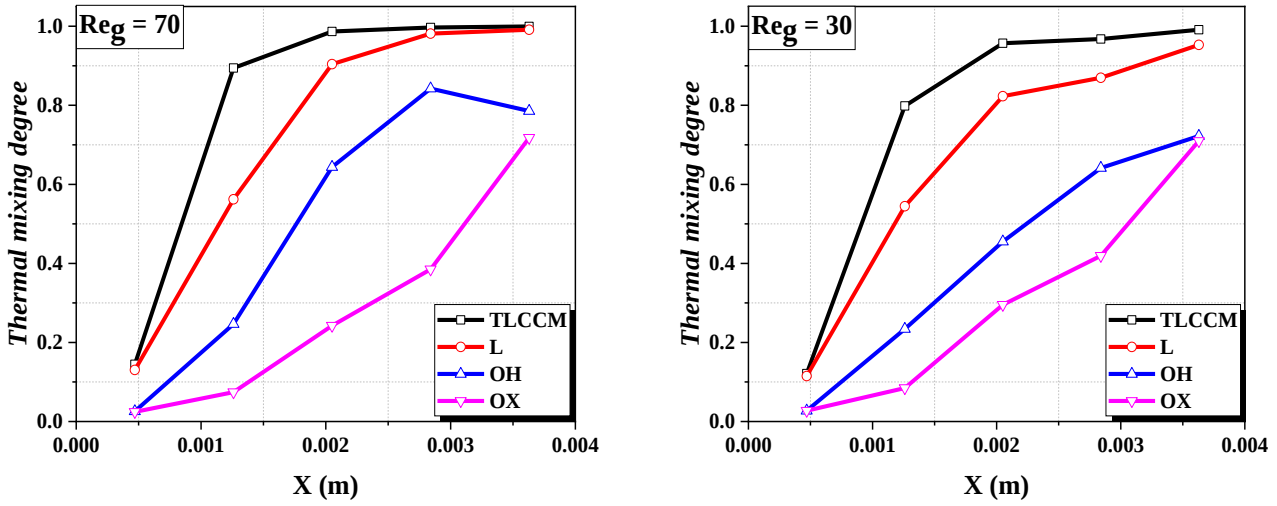

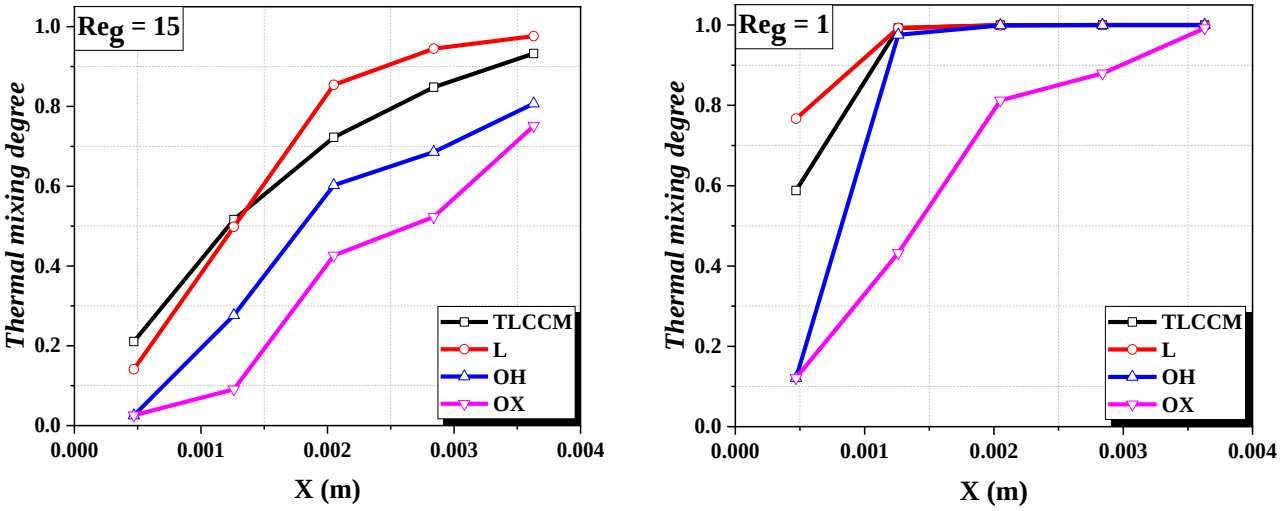

Fig. 10. Developments of the thermal mixing degree throughout the considered micromixers for n = 1.

Fig. 11 illustrates how the thermal mixing degree at the micromixers outlet varies with the generalized Reynolds number for different fluid behavior index values. The OH and OX micromixers consistently show poor thermal mixing performance throughout the entire range of generalized Reynolds numbers, regardless of the fluid behavior index. It's evident that the TLCCM micromixer undergoes a notable transition from diffusion regime to chaotic advection regime, with the critical generalized Reynolds number being 15. Furthermore, a rapid transition occurs between the two regimes within TLCCM micromixer, resulting in thermal mixing quality ranging from 0.9 to 0.99. These observations underscore the superior thermal mixing performance achieved using TLCCM micromixer.

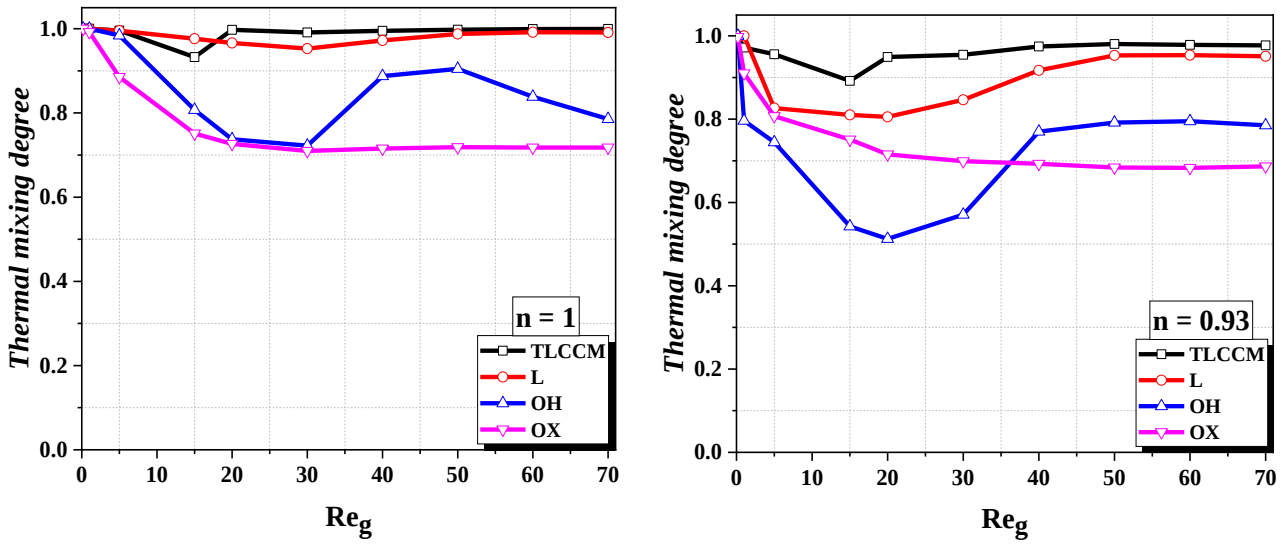

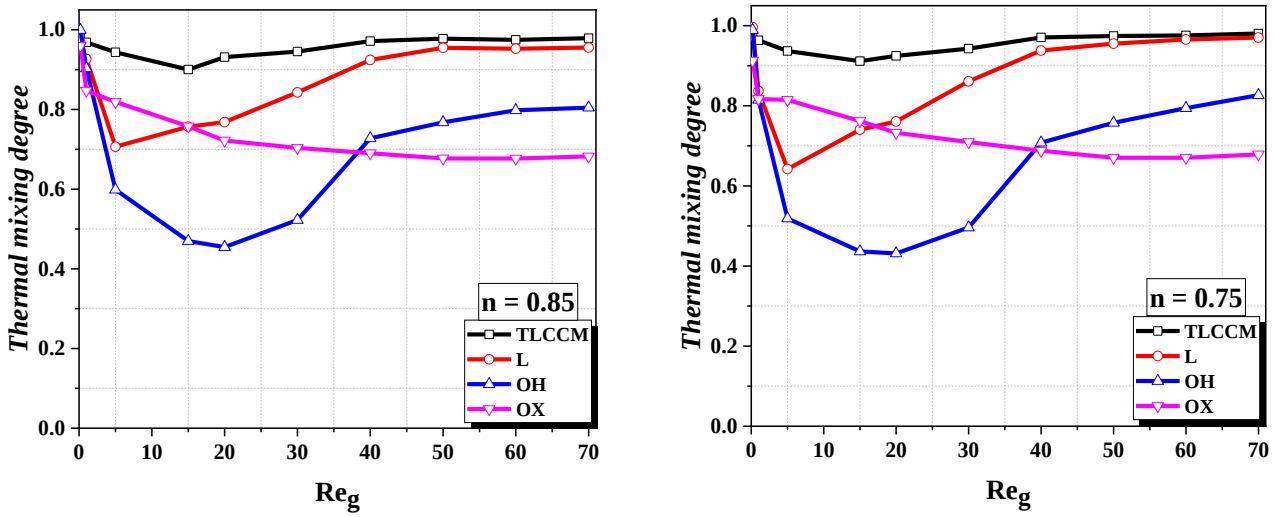

Fig. 11. Changes in thermal mixing degree at the micromixers outlet as a function of generalized Reynolds number, shown for various fluid behavior indices.

Fig. 12 shows how temperature profiles develop along the central line of the outlet plane for various micromixers. This is depicted at a generalized Reynolds number of 30, across the full range of fluid behavior indices. Significant fluctuations were observed for the OH, OX, and L micromixers between different temperature values with large intervals (between 306 K and 321 K), which explains the low thermal mixing quality obtained with these micromixers compared to the TLCCM micromixer. The latter presents a profile with very low fluctuations such that the mixing temperature evolves close to the desired mixing temperature value which is equal to 315 K.

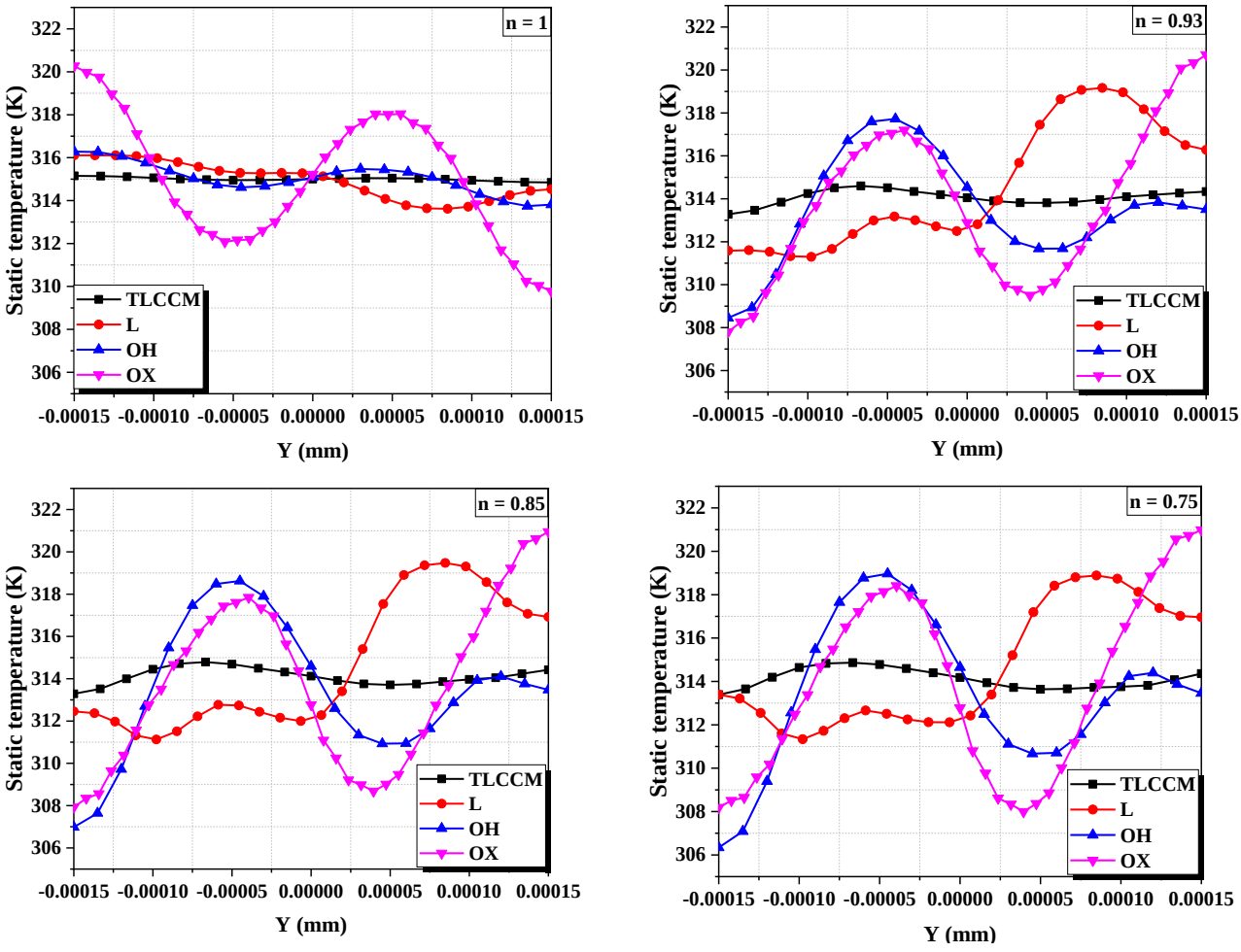

Fig. 12. Static temperature profiles at the mid-line of micromixers exit for different fluid behavior index (Re_g = 30).

Fig. 13 which presents the temperature distribution contours on the mid-plane along the micromixers makes it possible to visualize the obtained thermal mixing quality within the considered micromixers, for two values of fluid behavior index (n = 0.75 and 1) and for three values of generalized Reynolds number (Re_g = 1, 30, and 70).

The thermal mixing quality obtained using TLCCM micromixer is the best compared to the other three micromixers. The difference appears clearly in the state of pseudo-plastic fluids where the thermal mixing is improved from the second crossing of TLCCM micromixer. For Newtonian fluids with low Reynolds number (molecular diffusion regime), all micromixers exhibit high thermal mixing performances compared to the chaotic regime, where TLCCM micromixer exhibits the best mixing efficiencies.

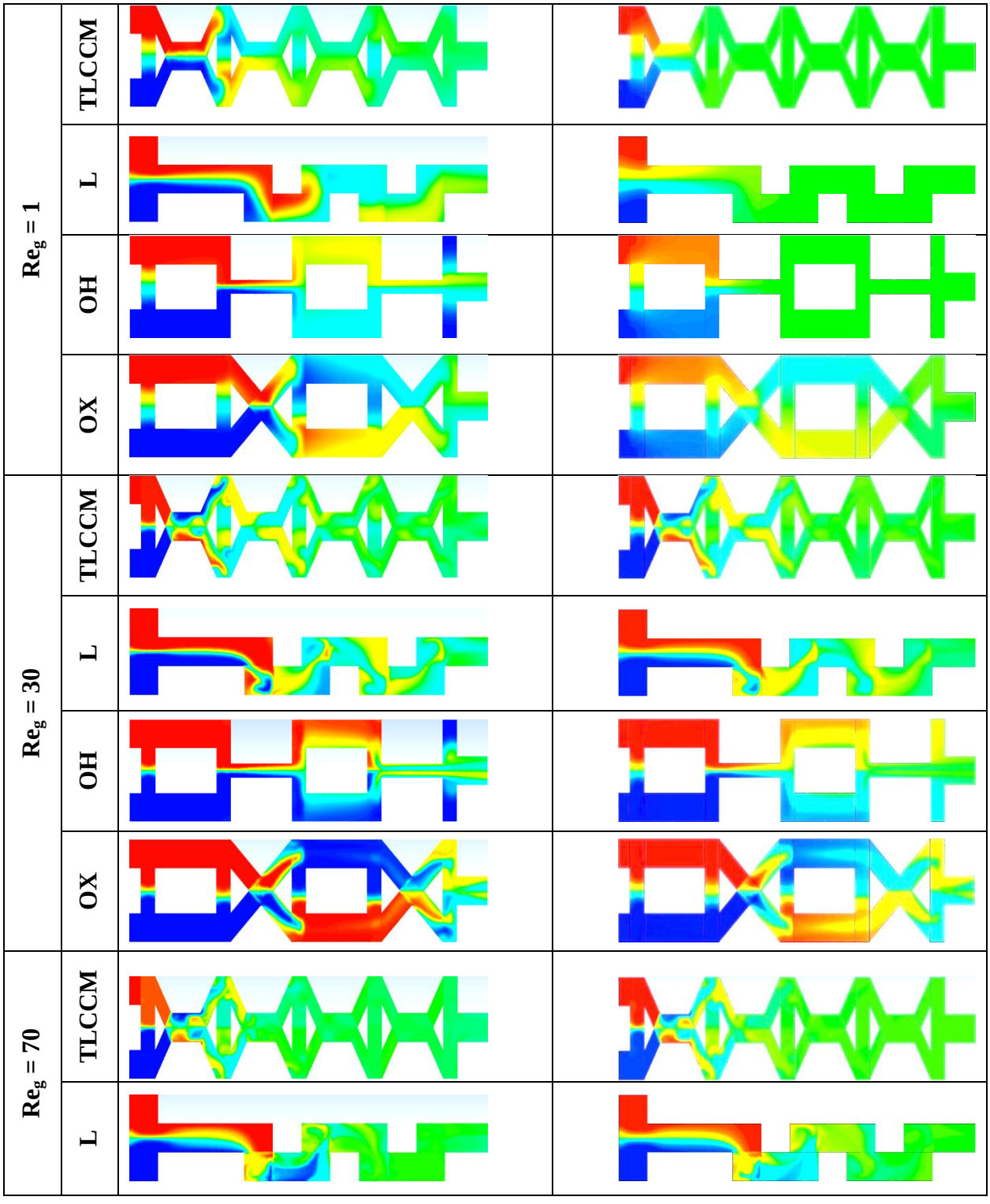

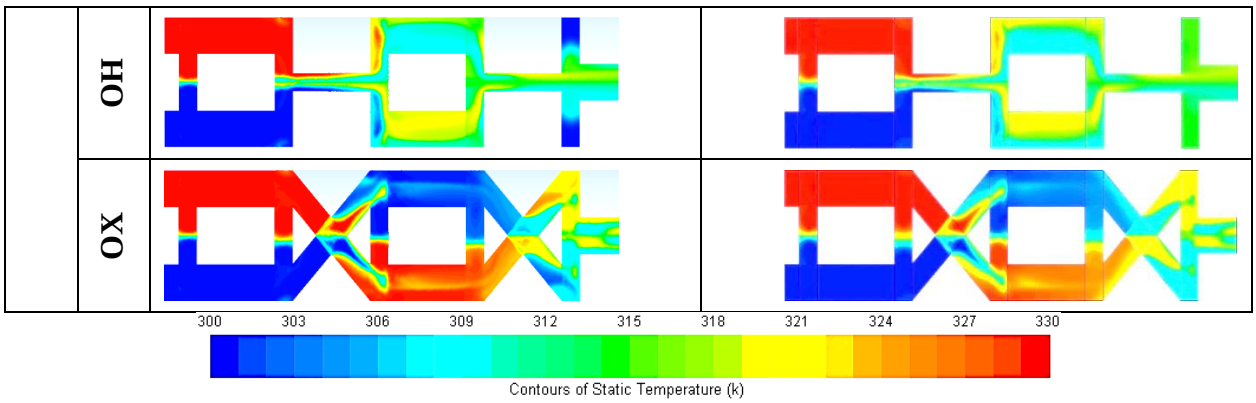

Fig. 13. Static temperature contours on a mid-plane of different micromixers: (left) n = 0.75; (right) n = 1.

Fig. 14 displays the temperature distribution contours at the outlet planes of various micromixers. These are shown across the full range of considered fluid behavior indices and for three generalized Reynolds number values (Re_g = 1, 30, and 70). A comprehensive view of these contours supports the previously presented results and analyses. Specifically, it confirms the superior performance of the TLCCM micromixer in both flow regimes, regardless of the fluid nature.

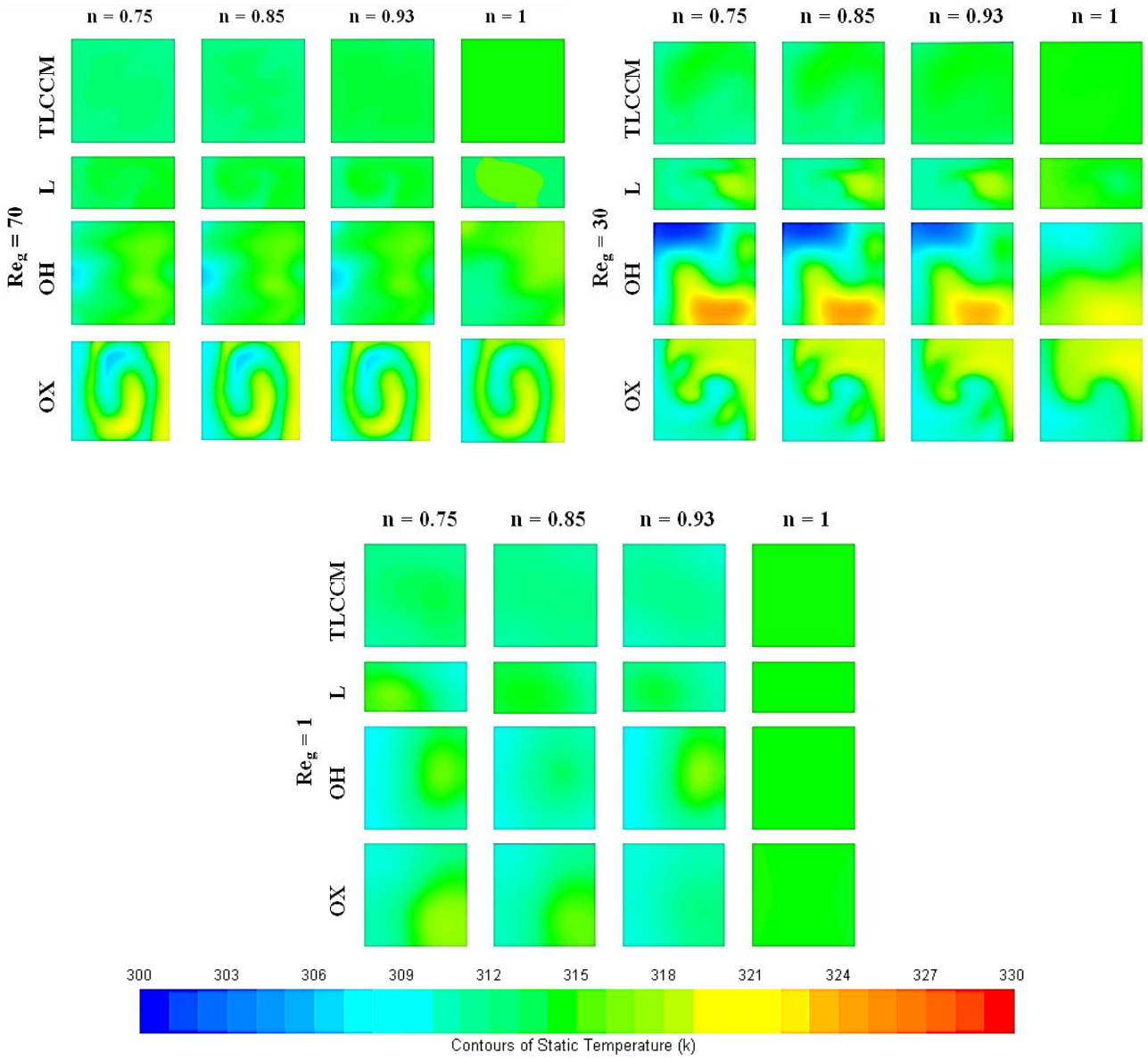

Fig. 14. Contours of static temperature at the exit of the examined micromixers for various fluid behavior indices.

4.4 Second law of thermodynamics and thermal efficiency in studied micromixers

Entropy generation is an energy degradation which occurs when the energy is transformed into heat or exchanged between two fluid species at different temperatures. The entropy generation accompanied with fluid flow is induced by viscous and thermal mechanisms, involving velocity and temperature gradients. The thermal mixing performances within the studied micromixers, including these several modes of flows, are closely related to the decreasing of the entropy generation. Therefore this constitutes sufficient motivation for a better knowledge and deep analysis of different mechanisms related to the creation of this entropy.

Fig. 15 illustrates the entropy generation linked to the thermal mixing versus generalized Reynolds number for different fluid behavior indexes. This figure illustrates the overall evolution of the entropy generation due to thermal mixing, for the different proposed micromixers: TLCCM, L, OH, and OX. It's found that for the TLCCM micromixer, the entropy generation linked to heat transfer in all cases of pseudo-plastic fluids is lower than the other micromixers and its value reduces with the increasing of fluid behavior index. While generalized Reynolds number is high, the entropy generation becomes higher. These results confirm once again that chaotic advection phenomenon constitutes a key parameter to improve the thermal mixing performances linked to the heat transfer and in particular when reducing generalized Reynolds number and increasing the fluid behavior index. Maximum entropy generation occurs in the case of pseudo-plastic fluids with low fluid behavior index (n = 0.75). These results also demonstrate that during the thermal mixing, the entropy created in TLCCM micromixer is the least significant compared to the other micromixers. Therefore, the minimum entropy generation leads to low thermal energy degradation.

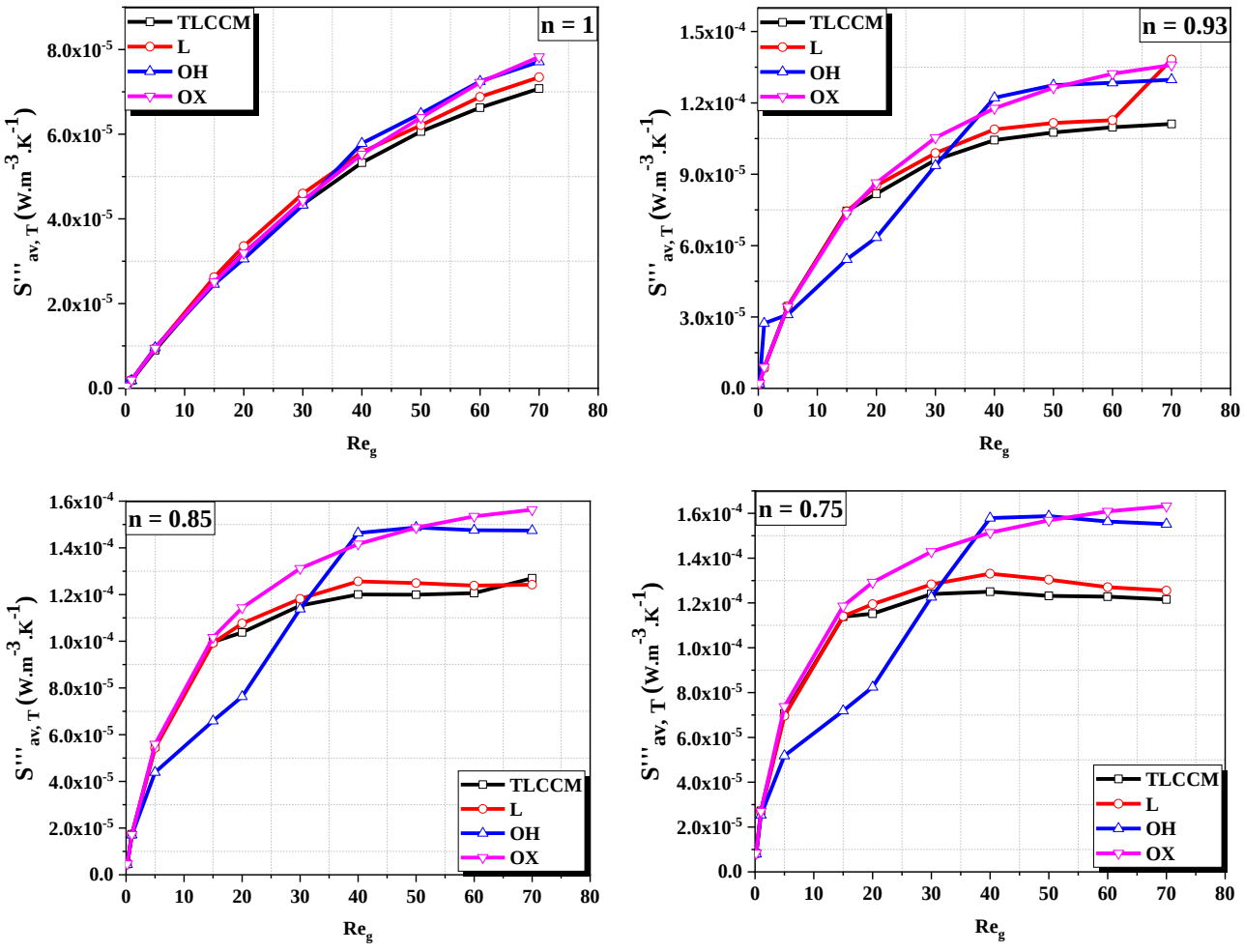

Fig. 15. Entropy generation variation associated with heat transfer ($S'''_{av,T}$) versus generalized Reynolds number for various fluid behavior index.

Fig. 16 presents the impact of the generalized Reynolds number on entropy generation rate linked to the pressure drops for the considered micromixers, for several fluid behavior index values. When the fluid behavior index increases, the entropy generation obviously reduces. However, the effects of generalized Reynolds number, which can be detected for all micromixers are relatively important. It could be noted that the evolution curves of entropy generation rate of all micromixers are dissimilar. The same observation is noticed for the entire range of the fluid behavior index. In particular, it could be seen clearly that entropy generation linked to the pressure drops presents slightly higher values with the TLCCM micromixer than that observed with the other micromixers. In addition, the entropy created linked to the pressure drops is very small, this is true in the case of a laminar regime particularly for creeping flows.

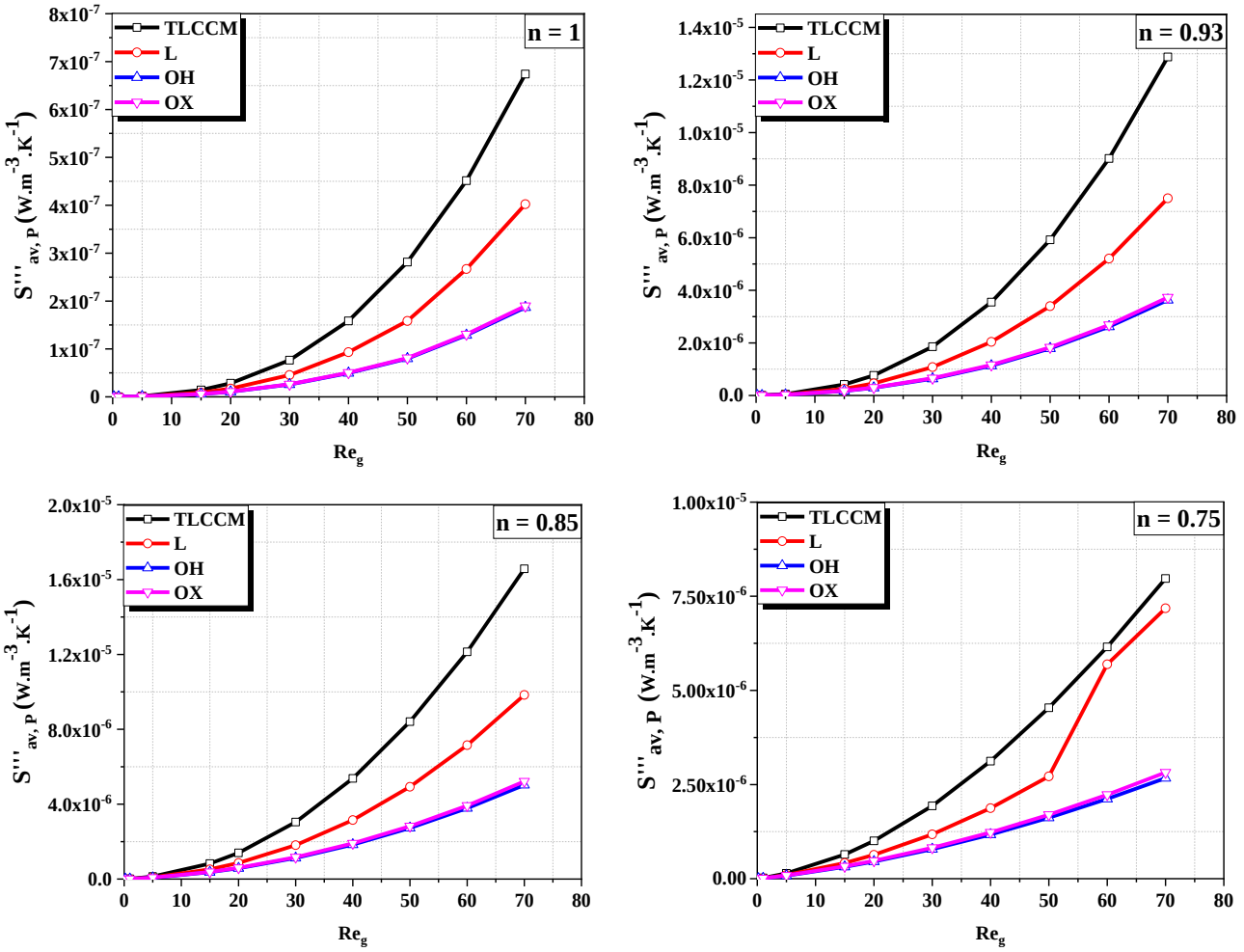

Fig. 16. Variation of the entropy generation linked to the pressure drops ($S'''_{av,P}$) versus generalized Reynolds number for various fluid behavior index.

The changes of global entropy generation versus generalized Reynolds number with different fluid behavior index are reported in Fig. 17. For all micromixers, the global entropy generation increases with generalized Reynolds number increasing, but reduces as the fluid behavior index increases. The cause for this trend is the fact that temperature gradients within the flow increase and are more dominant compared to pressure gradients. Furthermore, the overall entropy generation rate in three micromixers: L, OH and OX is higher than that for TLCCM micromixer, which leads to the enhancement of thermal mixing efficiency of TLCCM micromixer.

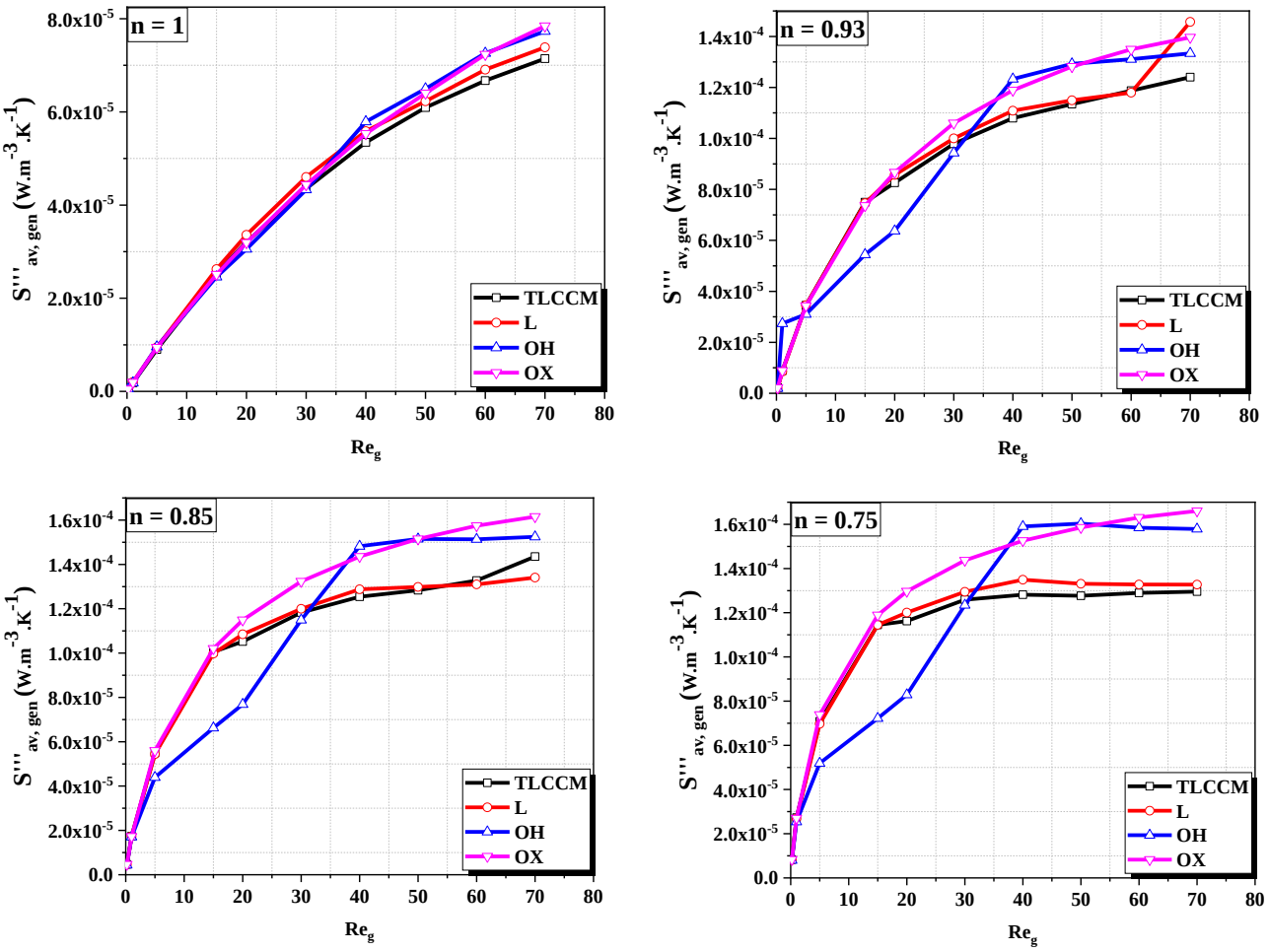

Fig. 17. Variation of the global entropy generation ($S'''_{av,gen}$) versus generalized Reynolds number for various fluid behavior index.

To check the importance of heat transfer entropy generation versus overall entropy generation in all proposed micromixers, Fig. 18 shows the changes of Bejan number with generalized Reynolds number for several fluid behavior indexes. For all micromixers, Bejan number values are greater than 0, and close to the upper limit, which is a credible result indicating that entropy generation is prevailed by irreversibility due to the heat transfer. This is because the effect of temperature gradients is greater than that of velocity gradients.

In our comparative study, the irreversibility due to fluid layers friction is less, which leads to a higher Bejan number in all micromixers, so entropy generation under existing flow conditions is prevailed by the irreversibility of heat transfer. Consequently, the TLCCM micromixer presents high mixing performances with low Reynolds numbers, whatever the fluid behavior index.

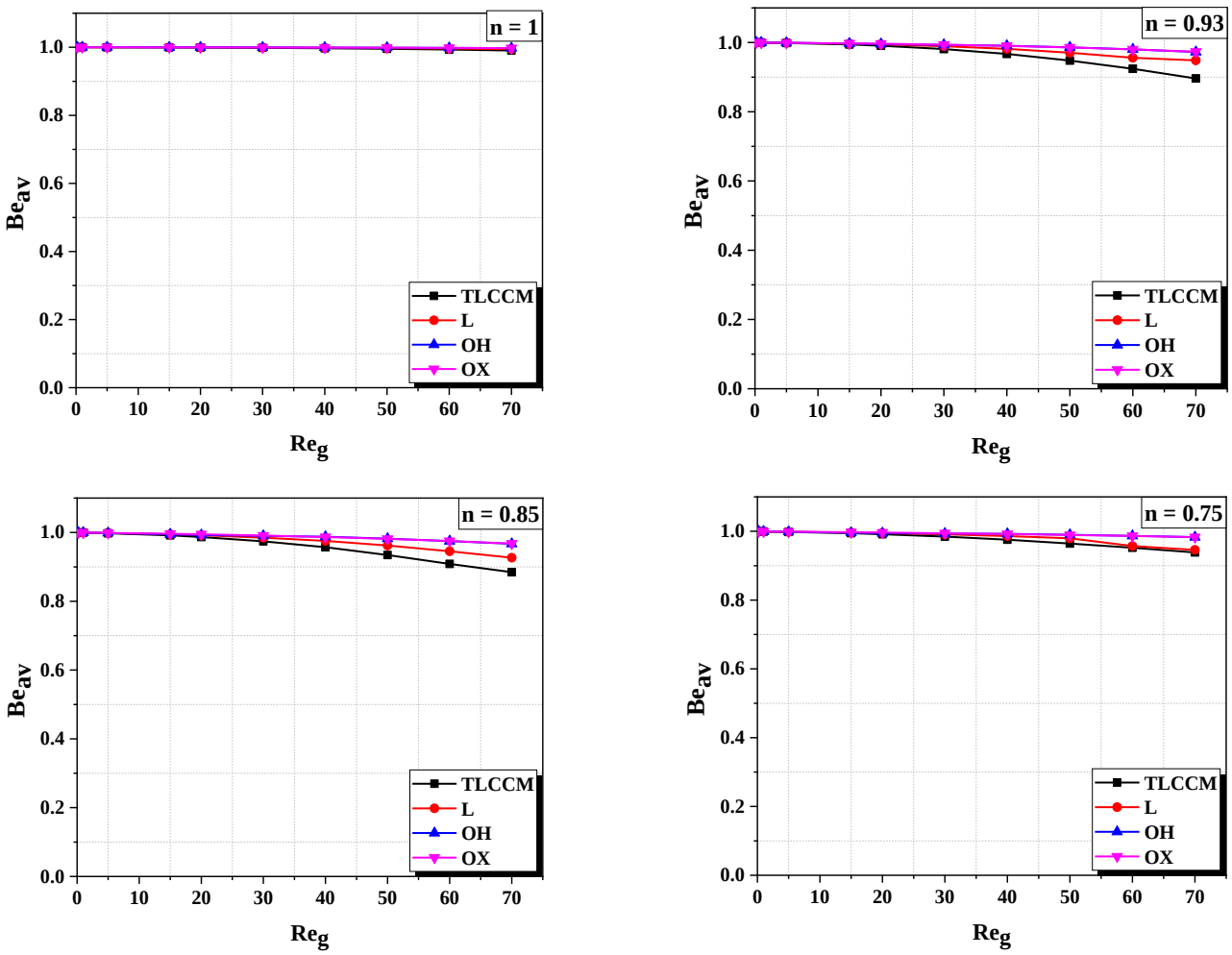

Fig. 18. Changes of average Bejan number versus generalized Reynolds number for various fluid behavior indexes.

The probability density function (PDF) plays a critical role in evaluating the uniformity of the temperature distribution downstream of the analyzed micromixers. Fig. 19 and Fig. 20 depict the PDF (%) at the exit section of each micromixer for two extreme fluid behavior index values (0.75 and 1), as well as for a vast range of generalized Reynolds numbers (1, 15, 30, and 70). The temperature profiles indicate that for L, OH, and OX micromixers, the temperature distribution at the exit section remains scattered across multiple temperature ranges, particularly for OH and OX micromixers, which exhibit bad mixing quality. This implies that using OH and OX micromixers for fluid mixing processes with low generalized Reynolds number may not be advisable. Conversely, the temperature distribution obtained for TLCCM micromixer distinctly differs from the other micromixers. As the hot and cold fluids traverse this micromixer, they undergo thorough mixing and tend to homogenize due to the chaotic advection within the TLCCM micromixer geometry. Consequently, the temperature distribution at the exit of TLCCM micromixer is tightly concentrated within a narrow range, with the peak of this distribution aligning with the desired mixing temperature of 315 K, regardless of the value of the fluid behavior index.

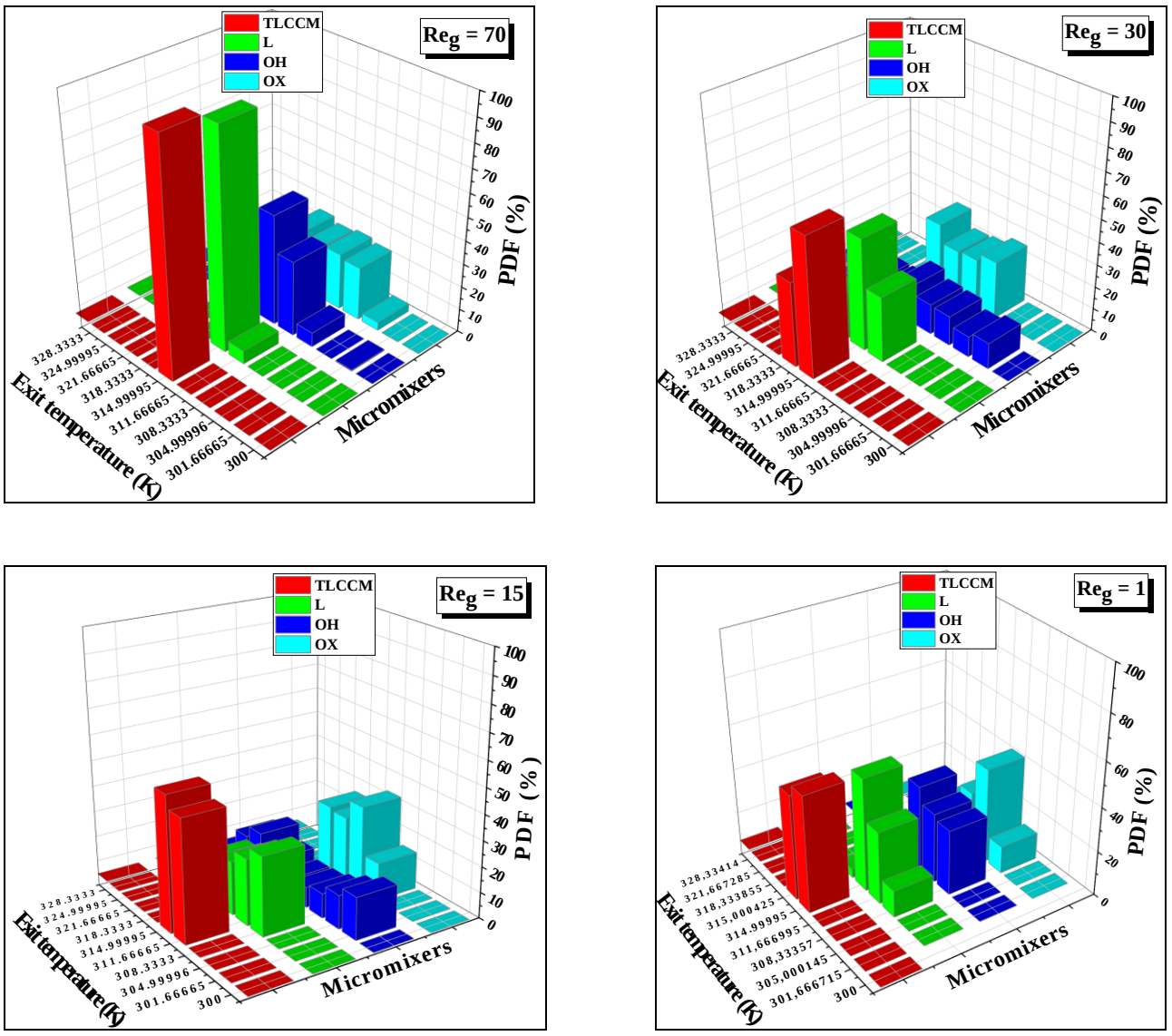

Fig. 19. Probability density function (PDF %) of temperature at the exit ~~TLCCM~~ of proposed micromixers ~~the exit~~ for several generalized Reynolds numbers with n = 0.75.

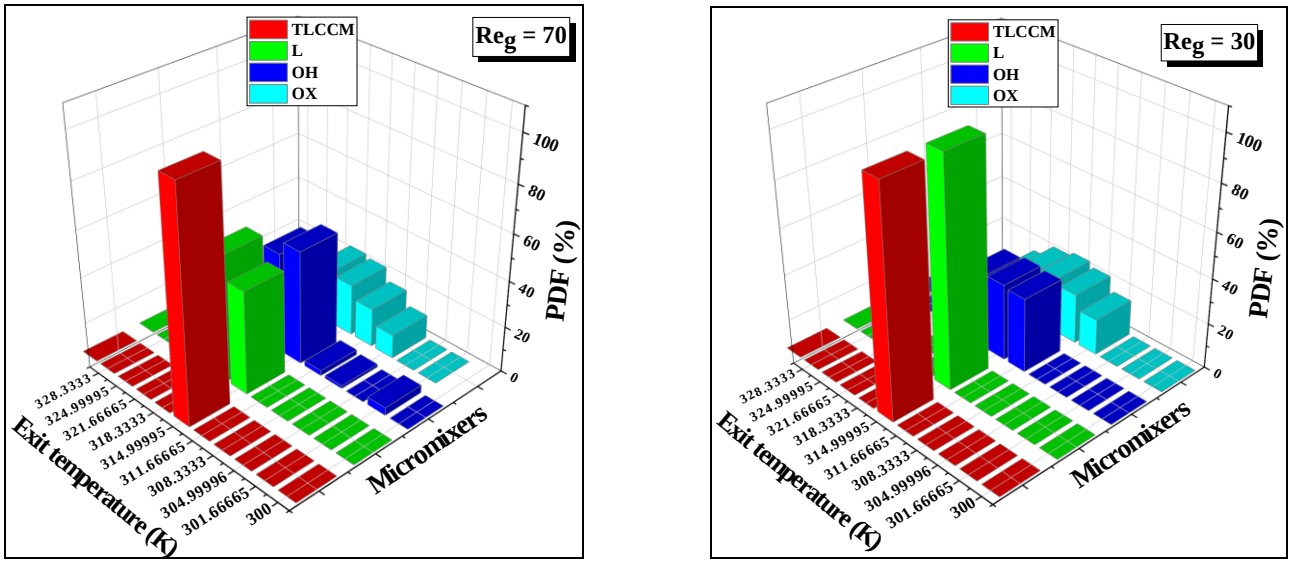

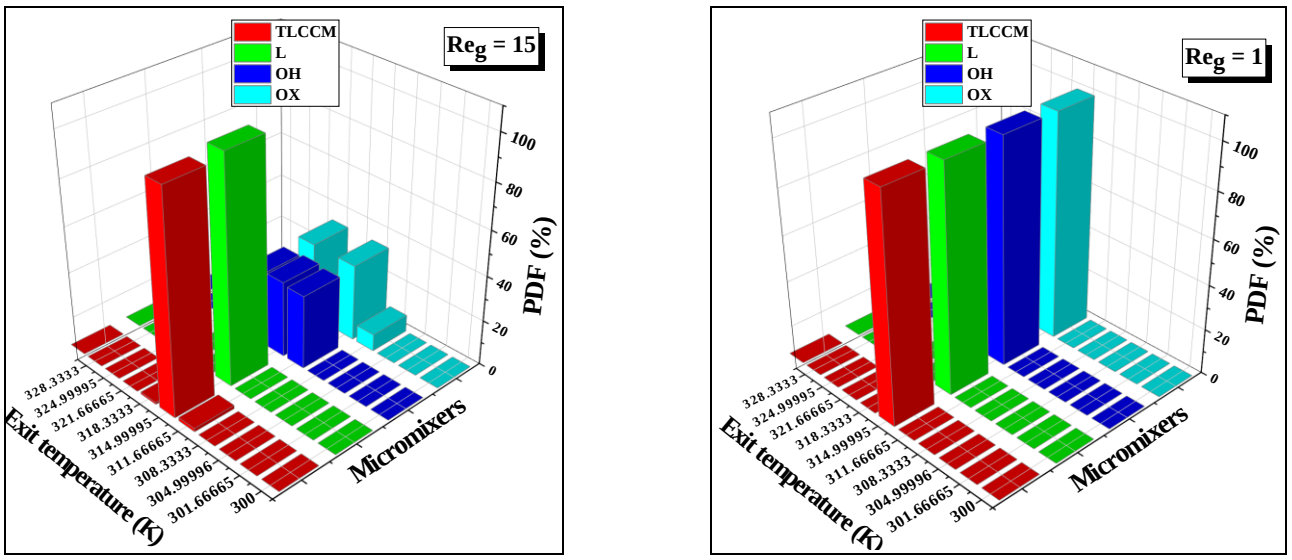

Fig. 20. Probability density function (PDF %) of temperature at the exit of ~~TLCCM~~ proposed micromixers ~~the exit~~ for several generalized Reynolds numbers with n = 1.

5. Conclusions

Microfluidics presents versatile and effective solutions for various practical applications across numerous industrial systems. However, achieving efficient thermal mixing at the microscopic scale remains challenging, primarily due to laminar flow regimes. Our focus was mainly directed towards developing tools capable of facilitating efficient thermal mixing at small scales using straightforward passive microdevices without the need for external actuation. The proposed micromixer employing division and recombination mechanisms was thoroughly examined. A comprehensive numerical investigation was conducted to analyze the thermal mixing efficiency, entropy generation, and temperature homogenization of pseudo-plastic fluids in four micromixers: TLCCM, L, OH, and OX. This investigation covered vast generalized Reynolds numbers range (from 1 to 70) and fluid behavior index values ranging from 0.75 to 1. TLCCM micromixer showcases robust heat exchange capabilities attributed to compression and stretching mechanisms, outperforming other conventional micromixers. This superiority stems from the chaotic advection phenomenon inherent in its geometry, providing an additional advantage for enhancing thermal mixing performance. TLCCM micromixer demonstrates significant enhancements in heat transfer, both quantitatively and qualitatively, resulting in increasingly homogeneous temperature distributions.

Consequently, entropy generation in this micromixer is primarily dominated by irreversibilities associated with heat transfer processes. The thermal mixing quality is assessed by two criteria: the thermal mixing degree (TMD) and the probability density function (PDF). Both criteria confirm that TLCCM micromixer excels in temperature uniformity of pseudo-plastic fluids. The assessement of the thermal mixing degree indicates that TLCCM micromixer achieves homogeneous mixing, approaching the maximum value of TMD. Additionally, analysis of the PDF reveals that the temperature map at the outlet plane of TLCCM micromixer is focused within a single interval, with the peak of this distribution corresponding to the wanted mixing temperature, regardless of the fluid behavior index value. In contrast, temperature map values at the outlet section of other micromixers are widely dispersed.

6. References

[1] J.P. Simoneau, J. Champigny, O. Gelineau, Applications of large eddy simulations in nuclear field, Nucl. Eng. Des. 240 (2010) 429–439.

[2] K.Y. Lee, S. Park, Y.R. Lee, S.K. Chung, Magnetic droplet microfluidic system in corporated with acoustic excitation for mixing enhancement, Sens. Actuators A: Phys. 243 (2016) 59–65.

[3] X. Guo, Y. Fan, L. Luo, Mixing performance assessment of a multi-channel mini heat exchanger reactor with arborescent distributor and collector, Chem. Eng. J. 227 (2013) 116–127.

[4] T. Sprogies, J.M. Köhler, G.A. Groß, Evaluation of static micromixers for flow-through extraction by emulsification, Chem. Eng. J. 135S (2008)S199–S202.

[5] M. Cho, S. Chung, Y.T. Kim, J.H. Jung, D.H. Kim, T.S. Seo, A fully integrated microdevice for biobarcode assay based biological agent detection, Lab Chip15 (2015) 2744–2748.

[6] K. Matsuyama, K. Mine, H. Kubo, K. Mae, Design of micromixer for emulsification and application to conventional commercial plant for cosmetic, Chem. Eng. J. 167 (2011) 727–733.

[7] L. Qiu, K. Wang, S. Zhu, Y. Lu, G. Luo, Kinetics study of acrylic acidpolymerization with a microreactor platform, Chem. Eng. J. 284 (2016)233–239.

[8] G. S. Kumar , R. N. Behera, Multi-objective optimization of a pipe energy pile with heat exchanger pipes subjected to chaotic advection, Journal of Energy Storage 81 (2024) 110413 1-13.

[9] E. Younes, Y. Moguen, K. El Omari, T. Burghelea, Y. Le Guer, C. Castelain, Experimental study of chaotic flow and mixing of Newtonian fluid in a rotating arc-wall mixer, International Journal of Heat and Mass Transfer, 187 (2022) 122459.

[10] E. Tripathi, P. K. Patowari, S. Pati, Comparative assessments of mixing and pressure drop characteristics in spiral, serpentine and straight micromixers, Meccanica 58 (2023) 1315‑1327.

[11] K. El Omari, Y. Le Guer, Thermal chaotic mixing of power-law fluids in a mixer with alternately rotating walls, J. Non-Newtonian Fluid Mech. 165 (2010) 641–651.

[12] A. Rahimzadeh, F. Ein-Mozaffari, A. Lohi, Scale-up study of aerated coaxial mixing reactors containing non-newtonian power-law fluids: Analysis of gas holdup, cavity size, and power consumption, Journal of Industrial and Engineering Chemistry, 113 (2022) 293–315.

[13] S. Wang, P. Wang, J. Yuan, J. Liu, Q. Si, D. Li, Simulation Analysis of Power consumption and Mixing Time of Pseudoplastic Non-Newtonian Fluids with a Propeller Agitator, Energies, 15 (4561) (2022) 1–24.

[14] A. Shiue, L. Zhu, C. L. Wang, J. C. Jeng, G. Leggett, Mixing performance of a non-Newtonian fluid in a coaxial agitated impeller reactor, Journal of the Taiwan Institute of Chemical Engineers, 143 (2023) 104715 1–17.

[15]X. Chen, T. Li, A novel passive micromixer designed by applying an optimization algorithm to the zigzag microchannel, Chemical Engineering Journal, 313 (2017) 1406–1414.

[16]X. Chen,and X. Chen, A novel electrophoretic assisted hydrophobic microdevice for enhancing blood cell sorting: design and numerical simulation, Analytical methods: advancing methods and applications, 16 (2024) 2368–2377.

[~~15~~17] W. Raza, S. Hossain, K. Y. Kim, A Review of Passive Micromixers with a Comparative Analysis. Micromachines, 11 (2020) 455 1–25.

[~~16~~18] J. Wang, Y. Li, H. Liu, G. Sun, X. Chen, T. Lang, R. Wang, B. Cui, H. Yuan, A 3D passive micromixer with particle of stochastic motion through limonene dissolution method, AIP Advances,; 11 (10) (2021) 105318.

[~~17~~19] L. Yan, S. Wang, Y, Cheng, Numerical Simulation of Mixing Process in a Splitting-and- Recombination Microreactor, Front. Chem. Eng. 3:803861(2022) 1–12.

[~~18~~20] C. Srisamran, S. Devahastin, Numerical simulation of flow and mixing behavior of impinging streams of shear-thinning fluids, Chem. Eng. Sci. 61 (2006) 4884–4892.

[~~19~~21] D. Mendels, E.M. Graham, S.W. Magennis, A.C. Jones, F. Mendels, Quantitative comparison of thermal and solutal transport in a T-mixer by FLIM and CFD, Microfluid Nanofluid. 5 (2008) 603–617.

[~~20~~22] P.R. Mashaei, S.M. Hosseinalipour, K. Esmailpour, Numerical investigation of thermal mixing of shear thinning fluids in one-way opposing jets, J. Comp. App. Res. Mech. Eng. 3(2)(2014) 95–103.

[~~21~~23] H. Luo, A. Delache, S. Simoëns, Direct Numerical simulation of a shear-thinning fluid in a T-junction cross flow, 24ème Cong. Fran. Méc. (2019)1–5.

[~~22~~24] A. Maurya, N. Tiwari, R.P. Chhabra, Thermal mixing of impinging laminar streams of shear-thinning fluids. Heat. Trans. Eng. (2019). 1–20.

[~~23~~25] A. Bejan, Entropy Generation Through Heat and Fluid Flow, Wiley, New York, 1982.

[~~24~~26] A. Bejan, Entropy Generation Minimization, CRC Press, Boca Raton, FL, 1996.

[~~25~~27] B. S. Yilbas, S. Z. Shuja, M. O. Budair, Second law analysis of a swirling flow in a circular duct with restriction, International Journal of Heat and Mass Transfer, 42 (1999) 4027–4041.

[~~26~~28] V. Zimparov, Extended performance evaluation criteria for enhanced heat transfer surfaces: heat transfer through ducts with constant wall temperature, International Journal of Heat Mass Transfer, 43 (2000) 3137–3155.

[~~27~~29] A .Z. Sahin, Thermodynamics of laminar viscous flow through a duct subjected to constant heat flux, Energy, 21(12) (1996) 1179–1187.

[~~28~~30] A .Z. Sahin, Irreversibilities in various duct geometries with constant wall heat flux and laminar flow, Energy, 23(6) (1998) 465–473.

[~~29~~31] T. H. Ko, Numerical analysis of entropy generation and optimal Reynolds number for developing laminar forced convection in double-sine ducts with various aspect ratios, International Journal of Heat and Mass Transfer, 49 (2006) 718–726.

[~~30~~32] T. H. Ko, K. Ting, Entropy generation and optimal analysis for laminar forced convection in curved rectangular ducts: A numerical study, International Journal of Thermal Sciences, 45 (2006) 138–150.

[~~31~~33] V. Zimparov, A. K. Silva, A. Bejan, Thermodynamic optimization of tree-shaped flow geometries, International Journal of Heat Mass Transfer, 49 (2006) 1619–1630.

[~~32~~34] J. C. Kurnia, A. P.Sasmito, T. Shamim, A. S. Mujumdar, Numerical investigation of heat transfer and entropy generation of laminar flow in helical tubes with various cross sections, Applied Thermal Engineering, 102 (2016) 849–860.

[~~33~~35] K. Yang, D. Zhang, Y. Xie, G. Xie, Heat Transfer and Entropy Generation of Non-Newtonian Laminar Flow in Microchannels with Four Flow Control Structures, Entropy, 18(302) (2016). 1–19.

[~~34~~36] A. Kaood, A. ElDegwy, A. Aboulmagd, Hydrothermal and entropy generation performance of convergent tubes with various dimple shapes, International Journal of Thermal Sciences, 197 (2024) 108842 1–18.

[~~35~~37] H. M. Xia, S.Y.M. Wan, C. Shu, Y.T. Chew, Chaotic micromixers using two-layer crossing channels to exhibit fast mixing at low Reynolds numbers, Lab on a Chip 5 (7) (2005) 748–755.

[~~36~~38] A. Kouadri, Y. Lasbet, M. Makhlouf, High mixing performances of shear-thinning fluids in two-layer crossing channels micromixer at very low Reynolds numbers, J. Mech. Eng. Sci., 13(4) (2019) 5938–5960.

[~~37~~39] A. Kouadri, E. Douroum, Y. Lasbet, T. T. Naas, S. Khelladi, M. Makhlouf, Comparative study of mixing behaviors using non-Newtonian fluid flows in passive micromixers, Int. J. Mech. Sci, 201 (2021)106472.

[~~38~~40] A. Kouadri, E. Douroum, S. Khelladi, Parametric study of the Crossing elongation effect on the mixing performances using short Two-Layer Crossing Channels Micromixer (TLCCM) geometry, Chem. Eng. Res. Design, 158 (2020) 33–43.

[~~39~~41] E. Douroum, S. Laouedj, A. Kouadri, T. T. Naas, S. Khelladi, A.Benazza, High hydrodynamic and thermal mixing performances of efficient chaotic micromixers: a comparative study, Chem. Eng. Proc: Proc. Int., 164 (108394) (2021) 1–19.

[~~40~~42] E. Douroum, A. Kouadri, A. Tahiri, M. Brihmat, S. Khelladi, Hydrodynamic and Kinematic Study to Analyze the Mixing Efficiency of Short Passive Micromixers, Ind. Eng. Chem. Res., 61 (17) (2022) 5994–6009.

[~~41~~43] T. Das, S. Chakraborty, Recent trends and future challenges, Biomicrofluidics, 34(4) (2009) 573–590.

[~~42~~44] F. T. Pinho, J. H. Whitelaw, Flow of non-Newtonian fluids in a pipe, J. Nonnewtonian Fluid Mech., 34 (1990) 129–144.

[~~43~~45] H. Fellouah, C. Castelain, A. Ould-El-Moctar, H. Peerhossaini, The Dean instability in power-law and Bingham fluids in a curved rectangular duct, J Nonnewtonian Fluid Mech, 165 (2010) 163–173.

[~~44~~46] F. Delplace , J. C. Leuliet, Generalized Reynolds number for the flow of power law fluids in cylindrical ducts of arbitrary cross-section, The Chem Eng J, 56 (1995) 33–37.

[~~45~~47] S. N. Li, H. N. Zhang, X. B. Li, Q. Li, F. C. Li, S. Qian, S. W. Joo, Numerical study on the heat transfer performance of non-Newtonian fluid flow in a manifold microchannel heat sink, Applied Thermal Engineering, , 115 (2017) 1213–1225.

[~~46~~48] S. Hossain, I. Lee, S.M. Kim,K.Y. Kim, A micromixer with two-layer serpentine crossing channels having excellent mixing performance at low Reynolds numbers, Chemical Engineering Journal, 327 (2017) 268–277.